Applied Catalysis B: Environmental 306 (2022) 121129

Contents lists available at ScienceDirect

Applied Catalysis B: Environmental

journal homepage: www.elsevier.com/locate/apcatb

Hydrogen production by steam reforming of propane and LPG over supported metal catalysts

Theodora Ramantani, Vissarion Evangeliou, George Kormentzas, Dimitris I. Kondarides *

Department of Chemical Engineering, University of Patras, GR-26504 Patras, Greece

ARTICLE INFO

Keywords:
Propane
LPG
Steam reforming
Hydrogen
TPO
Coke accumulation
Stability

ABSTRACT

The steam reforming of propane and LPG has been investigated over Ru, Rh, Ir, Pt, Pd and Re catalysts (1 wt%) dispersed on commercial metal oxide supports (Al_2O_3, TiO_2, CeO_2-ZrO_2). The Ru and Rh catalysts exhibit higher activity, which is comparable to that of a reference 10%Ni/Al_2O_3 sample. The performance of the Al_2O_3-supported Rh and 10%Ni catalysts deteriorates with time-on-stream due to the deposition of polymeric (C_β) and/or vermicular (C_V) carbon. The Ru-containing catalysts are considerably more stable because of the formation of small amounts of easily gasified carbon. Best results were obtained for the Ru/CeO_2-ZrO_2 catalyst, which is characterized by high activity, high selectivity toward H_2 and excellent stability with time-on-stream. This has been attributed to the formation of, mainly, monoatomic carbon (C_α) species under reaction conditions, the high efficiency of Ru to gasify carbon deposits, and the presence of labile lattice oxygen species on the CeO_2-ZrO_2 support.

1. Introduction

Hydrogen is a major feedstock for several chemical and petrochemical processes, including ammonia synthesis, methanol synthesis and hydrotreating in refineries, and a very attractive energy carrier that can be used for heating, transportation, and power generation with minimal emissions of greenhouse gases and hazardous compounds [1–5]. The demand for hydrogen is expected to grow considerably in the near future due to the widespread use of hydrogen-powered fuel cells for electricity generation, which represent a highly efficient and clean technology for mobile and small-to-medium scale stationary applications [6,7]. Industrially, hydrogen is economically produced from fossil fuels *via* steam reforming of hydrocarbons, mainly methane contained in natural gas, followed by the water-gas shift (WGS) reaction [1–4,8,9]. Renewable hydrogen can be produced from biomass-derived feedstocks [10,11] as well as *via* electrolysis of water using surplus electricity from renewable energy resources [12,13]. However, these technologies cannot currently guarantee a steady supply of hydrogen for the emerging applications. Consequently, the growing demand for hydrogen can only be met by using fossil fuels even if this is not a sustainable long-term option [9,14].

Hydrogen cannot be easily and economically stored and transported and, therefore, it must be produced on-site and on-demand, *e.g.*, for H_2 refueling stations and domestic applications, using a readily available fuel distribution infrastructure [15]. In this respect, natural gas may not the best option because natural gas pipelines are not available in many remote and less densely populated areas [15–18], especially in developing countries. An alternative and practical hydrogen source is liquefied petroleum gas (LPG), which is inexpensive, has a higher energy density than natural gas, can be easily and safely stored, and has a well-established distribution network even in areas where natural gas is not available [14,15,19–21]. Typically, LPG consists mainly of propane (C_3H_8) and butane (C_4H_{10}) in different proportions, depending on its source and processing methods [22], and exists in the liquid state under ambient temperature and moderate pressure.

Production of H_2 *via* steam reforming, partial oxidation, and autothermal reforming of propane [16,19–21,23–33] and LPG [14,15,17,34–42] has been studied to some extent in the literature. Among these routes, steam reforming (SR) has the advantage of delivering the highest hydrogen content in the reformate gas and is, therefore, more compatible with fuel cell applications. Steam reforming of LPG can be represented by the following endothermic reactions.

$$C_3H_8 + 3H_2O \rightarrow 3CO + 7H_2 \quad \Delta H^o = 498 \text{ kJ/mol} \tag{1}$$

$$C_4H_{10} + 4H_2O \rightarrow 4CO + 9H_2 \quad \Delta H^o = 650 \text{ kJ/mol} \tag{2}$$

* Corresponding author.
E-mail address: dimi@chemeng.upatras.gr (D.I. Kondarides).

https://doi.org/10.1016/j.apcatb.2022.121129
Received 24 September 2021; Received in revised form 28 December 2021; Accepted 20 January 2022
Available online 22 January 2022

which are accompanied by the moderately exothermic and thermodynamically limited WGS reaction:

$$CO+H_2O \leftrightarrow CO_2+H_2 \ \Delta H^o=-41.1 \text{ kJ/mol} \quad (3)$$

In addition to H_2 and carbon oxides (CO and CO_2), other compounds such as methane (CH_4), ethylene (C_2H_4) and ethane (C_2H_6) can be also produced *via* decomposition of reactants as well as *via* methanation of CO and/or CO_2:

$$CO+3H_2 \leftrightarrow CH_4 + H_2O \ \Delta H^o = -206 \text{ kJ/mol} \quad (4)$$

$$CO_2 + 4H_2 \leftrightarrow CH_4 + 2H_2O \ \Delta H^o = -165 \text{ kJ/mol} \quad (5)$$

Similar to other hydrocarbons, steam reforming of propane and butane is catalyzed by late transition metals (such as Ni and Cu) and precious metals (such as Ru, Rh and Pt), which are very active in breaking C-C and C-H bonds [1,2,9]. Nickel-based catalysts dispersed on metal oxide supports are widely used in industrial SR processes because of their fairly high activity and low cost and have been also tested for the title reactions [17,19,23–25,27,33,35–38,42]. However, these catalysts are easily deactivated due to coke deposition, which tends to be more severe for higher hydrocarbon feeds, including LPG [17,43]. Consequently, noble metal-containing catalysts, such as Rh [16,23,26,28,30,32,33,36,42,44], Pd [23,24,27,45], Pt [23,26,27,33,42,45], Ir [29,33] and Ru [27,33,42], have attracted significant interest in recent years as they are generally more active than Ni under propane and LPG reforming reaction conditions, and are characterized by a much lower tendency toward coke formation [43]. The limited availability and higher cost of these materials are partly compensated by their superior performance and the fact that much lower metal loadings are generally required to obtain activities and selectivities comparable to those of conventional Ni-based catalysts.

The catalytic performance and extent of coke accumulation during steam reforming reactions is known to depend strongly on the nature and characteristics of the support, which provides the sites for water adsorption and activation [2,23,43]. For example, the acidic sites of Al_2O_3 favor coke deposition, and the addition of promoters is necessary to improve water adsorption, mobility of OH species, and coke gasification [17,20,23]. On the other hand, the stability of precious-metal catalysts is enhanced when supported on reducible oxides, such as CeO_2 [17,23,30,33,36,42,45], TiO_2 [31,33,44], CeO_2-ZrO_2 [29,32,38,44] and YSZ [19,33], which exhibit good catalytic performance for fuel reforming reactions and enhanced resistance to deactivation due to coke accumulation. This has been attributed to the redox properties and high oxygen mobility of these materials, which promote water adsorption and activation as well as carbon removal from the catalyst surface under reaction conditions [17,36,38,45].

In the present work, the performance of six metal catalysts (Ru, Rh, Ir, Pt, Pd, Re) of the same loading (1 wt%) dispersed on three commercial supports (Al_2O_3, TiO_2, CeO_2-ZrO_2) is investigated for the steam reforming of propane and LPG, and is compared to that of a 10%Ni/Al_2O_3 catalyst used as reference material. The aim is to identify the metal-support combinations that are characterized by high activity and selectivity toward H_2, and, especially, stability with time-on-stream. In this respect, special emphasis is given to studying the nature and amount of carbon deposits accumulated on the catalyst surface following prolonged exposure to reaction conditions (40 h). Results show that the Ru/CeO_2-ZrO_2 catalyst exhibits the best performance for the steam reforming of both propane and LPG. The high stability of this catalyst with time-on-stream has been attributed to the ability of Ru to efficiently gasify active carbon deposits under reaction conditions which, when combined with the redox properties of the CeO_2-ZrO_2 support and the availability of highly labile lattice oxygen species, results in the suppression of coke accumulation that leads to catalyst deactivation.

2. Experimental

2.1. Catalyst preparation

Catalysts were prepared employing the wet impregnation method [46] using $Ni(NO_3)_2 \cdot 6H_2O$, $Ru(NO)(NO_3)_3$ (1.5%w/v Ru), N_3O_9Rh (10–15% w/w Rh), $(NH_3)_4Pt(OH)_2$ (8.6% w/w Pt), $IrCl_3$, $ReCl_5$ (Alfa Aesar), or $PdCl_2$ (Ventron Alfa Produkte) as metal precursor salts, and commercial Al_2O_3 (Aluminum oxide, catalyst support 99%, Alfa Aesar), TiO_2 (Degussa P25), or CeO_2-ZrO_2 (Cerium zirconium oxide 99.5%, Alfa Aesar) as supports. The slurries obtained after water evaporation were dried overnight at 100 °C and then reduced in H_2 flow at 300 °C (Rh, Pt, Pd), 400 °C (Ru, Ir), or 500 °C (Re, Ni) for 2 h. The resulting powders, denoted in the following as "fresh" catalysts, were stored in sealed vials for further use. The nominal metal loading of the catalysts thus prepared was 1 wt%, except for the reference Ni/Al_2O_3 catalyst whose metal loading was considerably higher (10 wt%).

2.2. Catalyst characterization

The specific surface areas (SSAs) of the fresh catalysts and of the samples collected after exposure to reaction conditions (denoted in the following as "used" catalysts) were determined according to the BET method with the use of a Micromeritics (Gemini III 2375) instrument. Powder X-Ray diffraction (XRD) patterns were obtained on a Brucker D8 Advance instrument. Transmission electron microscopy (TEM) images were recorded using a JEOL JEM-2100 model at 200 kV accelerating voltage. Details for the equipment and procedures used can be found elsewhere [47].

The metal dispersion of the fresh catalyst samples was estimated from hydrogen chemisorption measurements using the volumetric method [46,48]. Prior to each measurement, the catalyst sample (*ca.* 1.0 g) was pretreated by (a) dynamic vacuum at 250 °C for 1 h; (b) reduction with H_2 at 250 °C for 1 h, (c) evacuation for 30 min at 250 °C, and (d) cooling down to room temperature. Adsorption isotherms were obtained at 25 °C in the pressure range 0–75 Torr employing a modified Quantachrome Instruments (Autosorb iQ) analyzer. After obtaining the chemisorption isotherm, the weakly adsorbed hydrogen was removed from the catalyst surface by evacuating the adsorption cell for 10 min. A second isotherm was then obtained to determine the amount of reversibly chemisorbed hydrogen. The total hydrogen uptake and the reversible hydrogen uptake at monolayer coverage were obtained by extrapolating the corresponding adsorption isotherms to zero pressure. The irreversible hydrogen uptake was calculated from the difference between the latter two values [48].

2.3. Temperature-programmed experiments

Temperature-programmed desorption of hydrogen (H_2-TPD) and temperature-programmed oxidation (TPO) of coke deposits were carried out employing the apparatus and following the procedures described elsewhere [49]. In a typical H_2-TPD experiment, 100 mg of the catalyst sample were placed in a quartz microreactor, heated under He flow at 550 °C for 15 min, and then reduced *in situ* with flowing H_2 (30 cm^3 min^{-1}) at 300 °C (Rh, Pt, Pd), 400 °C (Ru, Ir), or 500 °C (Re, Ni) for 1 h. The sample was then purged with He at 550 °C for 15 min and subsequently cooled down to room temperature, where adsorption of hydrogen took place following interaction with a 3% H_2/He mixture (30 cm^3 min^{-1}) for 30 min. The gas stream was then switched to He and the temperature was increased to 750 °C with a heating rate of 10 °C min^{-1}. The hydrogen uptake was measured by integrating the H_2-TPD curve and was expressed in terms of the H/M ratio (where M denotes the dispersed metal).

The amount and reactivity toward oxygen of the carbon-containing species accumulated on the catalyst surface were assessed by TPO [50]. In a typical experiment, the catalyst sample collected after

exposure to reaction conditions was placed in a quartz microreactor and heated from room temperature to 750 °C under a 3% O_2/He flow with a heating rate of 10 °C min^{-1}. The amount of accumulated carbon was determined from the amount of CO_2 produced during the TPO experiment.

The analysis of reactants and products at the reactor effluent during the H_2-TPD and TPO experiments was accomplished employing an on-line mass spectrometer (Omnistar/ Pfeiffer Vacuum). The transient-MS signals at m/z = 2 (H_2), 18 (H_2O), 28 (CO), 32 (O_2), and/or 44 (CO_2) were continuously recorded. Responses of the mass spectrometer were calibrated against self-prepared mixtures of accurately known compositions.

2.4. Catalytic performance tests

The performance of the synthesized catalysts for the propane/LPG steam reforming reaction was evaluated at near atmospheric pressure using the apparatus and following the procedures that have been described in our previous work [51]. In a typical experiment, an amount of the fresh catalyst powder (100 mg) with particle size in the range 0.18 mm < d_p < 0.25 mm was placed in the reactor and reduced with H_2 at 300 °C (Rh, Pt, Pd), 400 °C (Ru, Ir), or 500 °C (Re, Ni) for 1 h. The temperature was then increased to 750 °C under flowing He and, after equilibration of the system, the flow was switched to the desired reaction mixture. The catalytic performance for the propane SR reaction was studied using a feed containing 2.3% C_3H_8 and 22.9% H_2O (balance He) at a total flow rate of 200 cm^3 min^{-1}. The SR of LPG was examined using a more concentrated feed consisting of 7.1% $C_3H_8 + C_4H_8$ and 68% H_2O (in He) and three propane:butane molar ratios (100:0; 95:5; 85:15), and a total flow rate of 270 cm^3 min^{-1}. In all cases the steam-to-carbon ratio (H_2O:C) was kept constant at 3:1. A small amount of Ar (0.7%) was always added to the feed as an internal standard to account for the volume change during the reaction [52]. The composition of the reformate at 750 °C was determined using the analysis system described elsewhere [51]. Similar measurements were then obtained following a stepwise lowering of temperature until the conversion of reactants dropped close to zero. Propane and butane conversions were calculated using the following expressions:

$$X_{C3H8} = \frac{[C_3H_8]_{in} - [C_3H_8]_{out}}{[C_3H_8]_{in}} \times 100 \quad (6)$$

$$X_{C4H10} = \frac{[C_4H_{10}]_{in} - [C_4H_{10}]_{out}}{[C_4H_{10}]_{in}} \times 100 \quad (7)$$

where $[C_3H_8]_{in}, [C_4H_{10}]_{in}$ and $[C_3H_8]_{out}, [C_4H_{10}]_{out}$ are the inlet and outlet concentrations of C_3H_8 and C_4H_{10}, respectively, obtained after correction for the volume change. Selectivities toward carbon-containing products (*e.g.*, CO, CO_2, CH_4, C_2H_4, C_2H_6) were calculated using the following expression, where n is the number of carbon atoms in the product i:

$$S_{C_i} = \frac{[C_i] \times n}{\sum([C_i] \times n)} \times 100 \quad (8)$$

Hydrogen selectivity was calculated using the equation

$$S_{H_2} = \frac{[H_2]}{[H_2] + \Sigma(y/2 \times [C_xH_y]i)} \times 100 \quad (9)$$

where y is the number of hydrogen atoms in the product i.

3. Results and discussion

3.1. Catalyst characterization

The specific surface areas of the unmetallized supports, the as-prepared catalysts and the used samples obtained after exposure to reaction conditions (Fig. 5, *vide infra*) are listed in Table 1. It is observed that the SSA of the fresh samples varies from one catalyst to another depending, mainly, on the specific surface area of the support (Al_2O_3:

Table 1
Characteristics of the supports and the synthesized catalysts.

Sample	Specific surface area[a] (m^2 g^{-1})		Metal dispersion (D)[b]	Apparent H/M ratio (from H_2-TPD)[c]	
	Fresh	Used		$(H/M)_{450}$	$(H/M)_{750}$
Al_2O_3	74	–	–	–	–
TiO_2	49	–	–	–	–
CeO_2-ZrO_2	13	–	–	–	–
10%Ni/Al_2O_3	57	65	0.03	0.04	0.10
Ru/Al_2O_3	68	60	0.17	0.40	0.59
Rh/Al_2O_3	73	59	0.65	0.79	1.03
Ir/Al_2O_3	74	64	0.31	0.03	0.29
Pt/Al_2O_3	74	62	0.43	0.45	1.66
Re/Al_2O_3	77	58	n.m.[d]	0.06	0.76
Pd/Al_2O_3	72	64	0.26	0.16	0.38
Ru/TiO_2	45	7	0.11	0.09	0.17
Rh/TiO_2	45	8	0.41	0.54	0.69
Ru/CeO_2-ZrO_2	14	13	0.46	3.48	3.92
Rh/CeO_2-ZrO_2	13	15	0.42	2.10	2.29

[a] SSA measured with the BET method.
[b] Metal dispersion estimated from irreversible hydrogen chemisorption using the volumetric method.
[c] The $(H/M)_{450}$ and $(H/M)_{750}$ ratios were calculated from H_2-TPD experiments based on the amounts of H_2 desorbed in the temperature ranges 25–450 °C and 25–750 °C, respectively.
[d] Not measured.

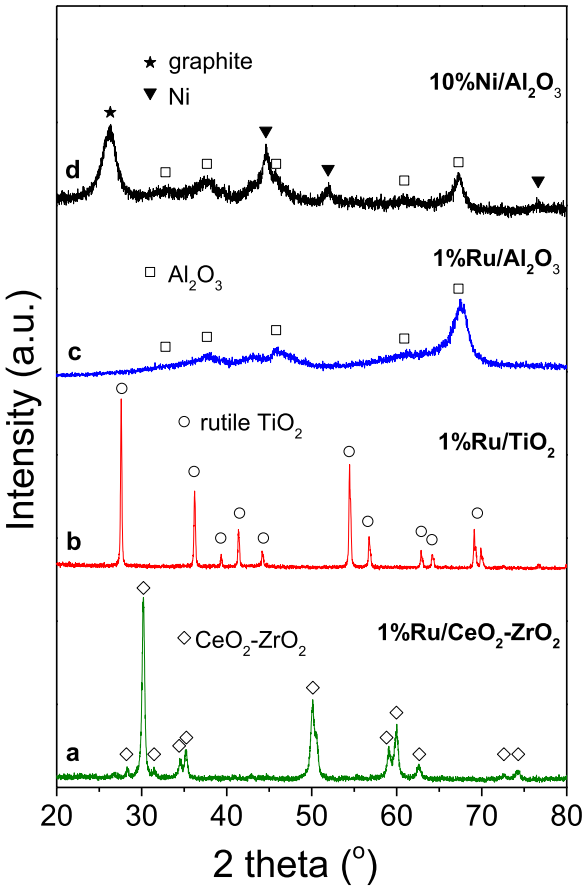

Fig. 1. Representative X-ray diffraction (XRD) patterns obtained over catalyst samples following exposed to reaction conditions (see Figs. 4–7): (a) 1%Ru/CeO_2-ZrO_2, (b) 1%Ru/TiO_2, (c) 1%Ru/Al_2O_3 and (d) 10%Ni/Al_2O_3.

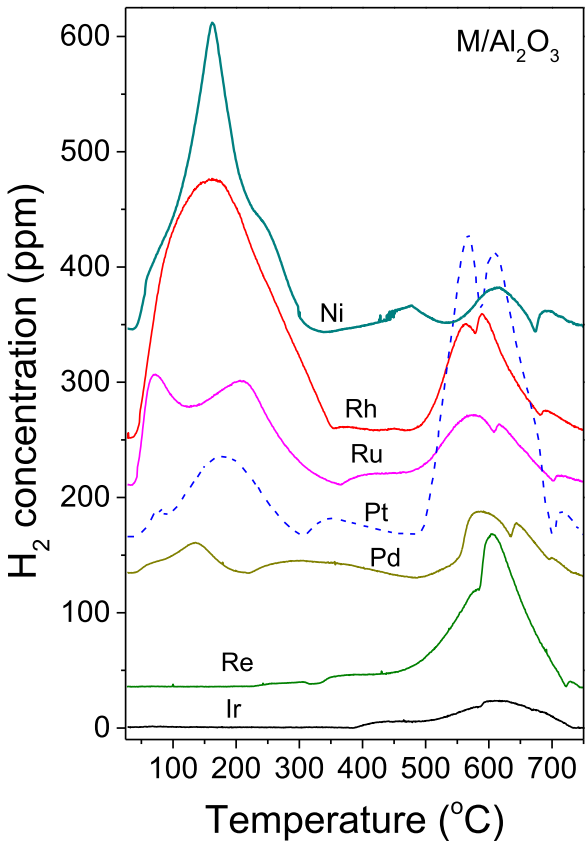

Fig. 2. Temperature-programmed desorption (H_2-TPD) profiles obtained for the indicated Al_2O_3-supported metal catalysts following interaction with H_2 at room temperature and subsequent heating ($\beta = 10$ °C min^{-1}) under He flow (30 cm^3 min^{-1}) at 750 °C.

74 m^2/g; TiO_2: 49 m^2/g; CeO_2-ZrO_2: 13 m^2/g) and to a lesser extent on the nature of the dispersed metal. The Al_2O_3-supported precious metal catalysts exhibit the highest SSA values (68–77 m^2 g^{-1}). The relatively lower specific surface area of the 10%Ni/Al_2O_3 catalyst (57 m^2 g^{-1}) can be attributed to the much higher metal loading of this sample, which may result in pore blocking. The SSAs of the two CeO_2-ZrO_2-supported catalysts (13–14 m^2 g^{-1}) and the two TiO_2-supported samples (45 m^2 g^{-1}) are similar with those of the corresponding bare supports. Exposure of the CeO_2-ZrO_2-supported catalysts to reaction conditions at temperatures up to 750 °C (Fig. 5, *vide infra*) does not affect, practically, their SSA. In contrast, this treatment results in a substantial decrease of the SSA of the two TiO_2-supported samples from 45 m^2 g^{-1} to 7–8 m^2 g^{-1}. This can be attributed to the phase transformation of TiO_2 from anatase to rutile (see Supplementary Information, Fig. S1), which is known to occur at temperatures higher than *ca.* 600 °C [47,53]. The Al_2O_3--supported samples also exhibit a decrease of SSA following exposure to reaction conditions, possibly due to particle growth and sintering of the support associated with the partial phase transformation of γ-Al_2O_3 to δ-alumina or θ-alumina, which is known to occur at high temperatures [54]. It is of interest to note that the SSA of the used 10%Ni/Al_2O_3 catalyst (65 m^2 g^{-1}) appears to be higher than that of the fresh sample (57 m^2 g^{-1}). This apparent increase of SSA is due to the formation of large amounts of coke following exposure of this sample to propane SR conditions at 750 °C and subsequent stepwise decrease of temperature to 400 °C (Fig. 5, *vide infra*). In fact, the mass of the used sample was measurably larger than that originally placed in the reactor, which was not the case for the rest of the catalysts investigated.

The phase composition of the fresh and used catalysts was studied with X-ray diffraction. In Fig. 1 are shown representative XRD patterns obtained for three used Ru catalysts, namely Ru/CeO_2-ZrO_2 (trace a), Ru/TiO_2 (trace b), and Ru/Al_2O_3 (trace c). It is observed that, in all cases, the diffractograms contain only reflections originating from the respective metal oxide support (XRD patterns of the unmetallized supports are not shown for brevity). The absence of XRD peaks attributable to the dispersed metals can be explained considering the low metal loading of these samples (1 wt%) and indicates the presence of relatively small Ru crystallites. Qualitatively similar results were obtained for all noble metal catalysts investigated (Supplementary Information, Fig. S1). In contrast, the XRD pattern obtained for the used 10%Ni/Al_2O_3 catalyst (Fig. 1, trace d) contains reflections at angles (2θ) of 44.6°, 51.9° and 76.6° attributable metallic Ni (JCPDS 4-850) as well as an intense peak at $2\theta = 26.3°$ associated with graphite carbon (JCPDS 41–1487). The latter reflection was absent in the XRD pattern of the fresh 10%Ni/Al_2O_3 catalyst indicating that exposure of this sample to reaction conditions results in the accumulation of significant amounts of carbon on the catalyst surface.

The values of metal dispersion (D) obtained from the measurements of irreversible hydrogen chemisorption at room temperature are listed in Table 1. It should be noted that we chose not to use the amounts of total hydrogen adsorption in these calculations because in several cases, especially for the CeO_2-ZrO_2 supported samples, the apparent H:M ratio was found to be higher than unity, indicating the occurrence of spillover phenomena.

To further investigate the interaction of hydrogen with the dispersed metal and the extent of hydrogen spillover on the support, H_2-TPD experiments were carried out over the freshly prepared catalysts. As shown in Fig. 2, the H_2-TPD profiles obtained for the Al_2O_3-supported catalysts are characterized by two desorption regions, one at temperatures in the range 25–450 °C and a second one at higher temperatures in the range 450–750 °C. According to results of previous studies obtained, for example, over Al_2O_3-supported Ni [55,56], Pd [57], Rh [58], and Pt [59] catalysts, the H_2 desorption peaks appearing at temperatures lower than *ca.* 450 °C are generally attributed to species adsorbed on sites located on the dispersed metal crystallites and/or at the metal-support interface while desorption features at temperatures higher than *ca.* 450 °C are due to spillover hydrogen associated with the support. As observed in Fig. 2, desorption peaks attributable to spillover hydrogen are present in the H_2-TPD curves of all M/Al_2O_3 catalysts investigated. The capability of Al_2O_3 to accommodate spillover hydrogen species has been related to the surface acidity of this support [57,58]. Regarding the relative intensity of desorption peaks attributed to spillover hydrogen, it depends appreciably on the nature of the dispersed metal (Fig. 2). This has been related to the different hydrogen diffusion coefficients of the metals, which affect the transfer of hydrogen from the metal to the support [57]. For example, the greater amounts of spillover hydrogen generated over Pd/Al_2O_3 compared to Ni/Al_2O_3 catalysts has been linked to the considerably higher diffusion coefficient of hydrogen on Pd (*ca.* 10^{-11} m^2 s^{-1}) relative to Ni (*ca.* 10^{-14} m^2 s^{-1}) ([57] and refs. therein).

The desorption curves presented in Fig. 2 were used to estimate the apparent $(H/M)_{750}$ ratios, which are based on the total amounts of H_2 desorbed in the H_2-TPD experiments, and the results obtained are listed in Table 1. It is observed that in the cases of the Rh/Al_2O_3 and Pt/Al_2O_3 catalysts the apparent $(H/M)_{750}$ ratios are higher than unity, providing additional evidence of the presence of spillover hydrogen. Consequently, the $(H/M)_{450}$ ratios, which are based on the amount of H_2 desorbed at temperatures lower than 450 °C, were also calculated to provide a more realistic picture of the metal dispersion. Results presented in Table 1 show that, in most cases, these values are in reasonable agreement with the dispersion values obtained from irreversible hydrogen chemisorption using the volumetric method. It should be noted, however, that the choice of the 25–450 °C temperature interval used for the calculation of the H/M ratios is rather arbitrary and may not correspond well to hydrogen chemisorbed on the metal surface for all catalysts investigated. This, combined with the different experimental conditions employed in the two methods (*i.e.* static/volumetric *vs.*

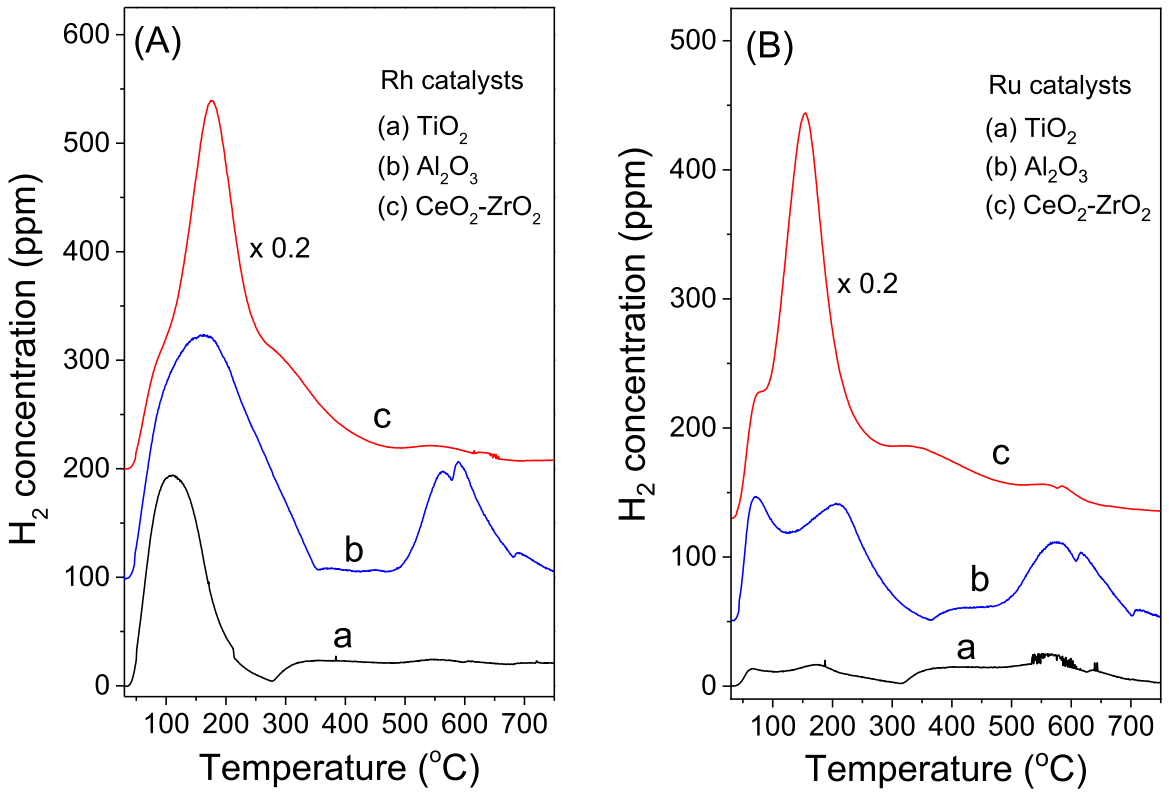

Fig. 3. Temperature-programmed desorption (H_2-TPD) profiles obtained for (A) Rh and (B) Ru catalysts dispersed on the indicated supports. Experimental conditions same as in Fig. 2.

dynamic hydrogen adsorption) may explain the relatively large differences in metal dispersion values obtained for certain samples (*e.g.*, Ru/Al_2O_3 and Ir/Al_2O_3).

The H_2-TPD profiles obtained for Rh and Ru catalysts dispersed on different supports (TiO_2, Al_2O_3, CeO_2-ZrO_2) are shown in Fig. 3 and the calculated H/M ratios are listed in Table 1. It is observed that the total amount of desorbed H_2 depends strongly on the nature of the support and, for both metals, $(H/M)_{750}$ decreases in the order CeO_2-$ZrO_2 \gg Al_2O_3 > TiO_2$. Interestingly, the $(H/M)_{450}$ ratios obtained for both Rh and Ru catalysts supported on CeO_2-ZrO_2 are much higher than unity (Table 1), indicating that a large part of the H_2 desorbing at temperatures lower than *ca.* 450 °C is due to species associated with the support. The presence of such species may be related to the partial reduction of the CeO_2-ZrO_2 support during the pretreatment of the catalysts samples with hydrogen before performing the H_2-TPD experiments. It has been reported, for example, that large amounts of hydrogen desorb from unmetallized, partially reduced $CeO_{2-\delta}$ samples in the temperature range 95–350 °C [60], which is in the same range where the intense TPD peaks appear for both the Rh/CeO_2-ZrO_2 and Ru/CeO_2-ZrO_2 samples (Fig. 3). The ability of CeO_2-supported noble metal catalysts, such as Rh/CeO_2, to chemisorb large amounts of hydrogen at room temperature has been reported by Bernal et al. [61] who concluded that, due to the occurrence of intense spillover phenomena, the experimental H/Rh values are much larger than those expected for true hydrogen adsorption on the metal. This justifies that the methodology used in the present work for the determination of the metal dispersion, which is based on the amount of irreversible hydrogen chemisorption, is reliable and overcomes the abovementioned problems and limitations.

Overall, results presented in Figs. 2 and 3 show that the adsorption characteristics and relative amounts of spilled-over hydrogen depend on the metal-support combination employed. As discussed by Amorim and Keane ([57] and refs. therein) the extent of spillover is influenced by several interrelated factors, including the number and nature of adsorption sites, the metal dispersion and the SSA of the support [62, 63], making it difficult to decouple such contributions and identify one dominant factor. Further investigation of these issues is beyond the scope of the present work and may be the subject of our future studies.

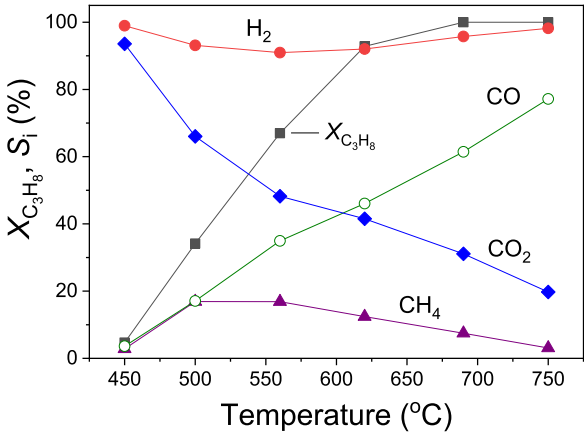

Fig. 4. Conversion of propane (X_{C3H8}) and selectivities to the indicated reaction products obtained over the 1%Ru/Al_2O_3 catalyst as a function of reaction temperature. Experimental conditions: mass of catalyst (*W*): 100 mg; particle diameter: $0.18 < d_p < 0.25$ mm; feed composition: 2.3% C_3H_8, 22.9% H_2O; 0.7% Ar (balance He); total flow rate (*F*): 200 cm^3 min^{-1}.

3.2. Steam reforming of propane

3.2.1. Effects of the nature of the dispersed metal

The effects of the nature of the dispersed metal on the catalytic performance for the propane SR reaction were examined over Al_2O_3-supported Ru, Rh, Ir, Pt, Pd, and Re catalysts (1 wt%), and results were compared to those of the reference 10%Ni/Al_2O_3 sample. Typical results

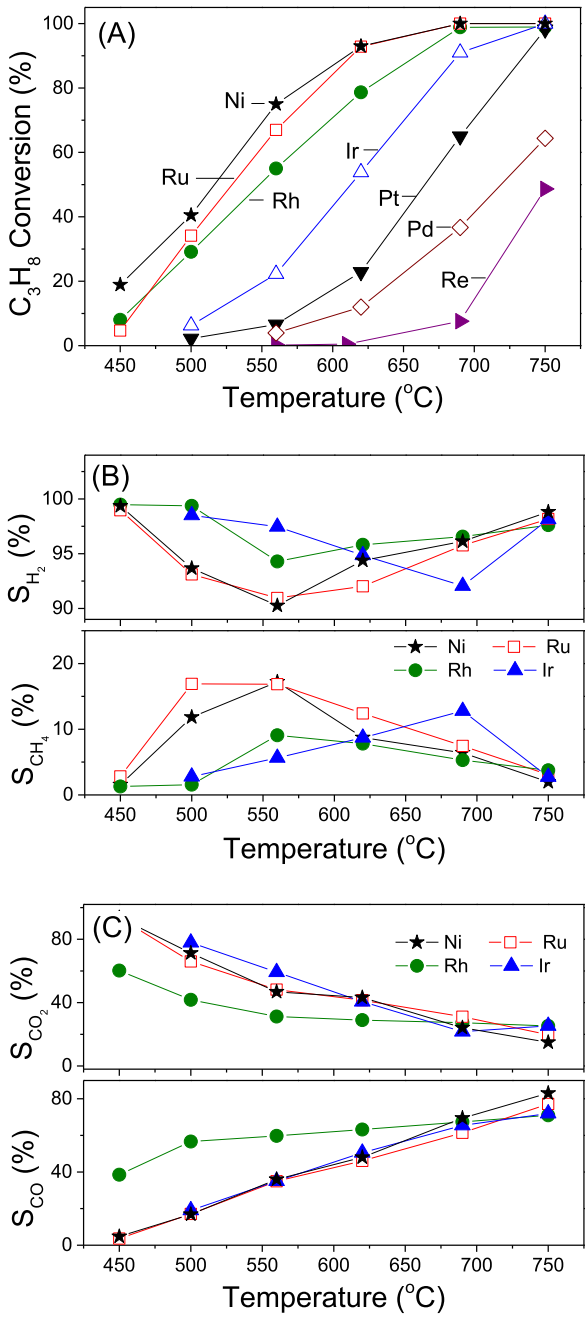

Fig. 5. (A) Conversion of propane, (B) selectivities to H_2 and CH_4, and (C) selectivities to CO_2 and CO obtained over the indicated Al_2O_3-supported metal catalysts. Experimental conditions: same as in Fig. 4.

obtained for the Ru/Al_2O_3 catalyst are shown in Fig. 4, where the conversion of propane (X_{C3H8}) and the selectivities to reaction products (S_i) are plotted as functions of reaction temperature. It is observed that the catalyst becomes active at temperatures around 450 °C. Conversion of propane increases progressively with the increase of temperature and reaches 100% at *ca.* 700 °C, where selectivity toward hydrogen is higher than 95%. Selectivity toward CO_2 decreases monotonically with increasing temperature while S_{CO} follows an opposite trend indicating the occurrence of the RWGS reaction, which is favored at higher temperatures. The major hydrogen-containing by-product formed is methane, with S_{CH4} passing through a maximum in the temperature range 500–550 °C. At higher temperatures, S_{CH4} progressively decreases because of the occurrence of the thermodynamically favored CH_4 steam reforming reaction. In addition to the above-mentioned products, negligible amounts of C_2H_4 and C_2H_6 were also detected (not shown for clarity).

Results of similar catalytic performance tests obtained over the rest of the Al_2O_3-supported metal catalysts investigated are presented in the Supplementary Information (Fig. S2). For comparison purposes, representative results are also shown in Fig. 5. It is observed that the 10%Ni catalyst exhibits the highest propane conversion values at temperatures lower than *ca.* 600 °C, with X_{C3H8} being close to 20% at 450 °C and reaching 100% at 690 °C (Fig. 5A). Ruthenium and rhodium are the most active noble metals studied, with the propane conversion curve of Ru/Al_2O_3 being comparable to that of the $10\%Ni/Al_2O_3$ catalyst. The conversion curves of Ir and Pt catalysts are shifted toward higher temperatures by *ca.* 100 °C and 150 °C, respectively, compared to that of 10%Ni. Finally, the Pd and Re catalysts are significantly less active, and temperatures higher than 700 °C are necessary to achieve propane conversions higher than 40%. This catalyst ranking is not much different than that reported for the propane SR reaction over Al_2O_3-supported metal catalysts [33] as well as for the SR of other hydrocarbons, such as ethane, on different supports [64]. For example, Kokka et al. [33] found that the propane SR activity of Al_2O_3-supported Rh, Ir and Ru (1 wt%) is higher than that of Pt and Re. Rostrup-Nielsen [64], showed that the relative activity of metals for the steam reforming of ethane at atmospheric pressure and 773 K follows the order Rh, Ru > Ni, Pd, Pt > Re, whereas a similar trend (Ru, Rh > Ir > Pt, Pd) has been reported by Qin et al. [65] for the steam and CO_2 reforming of CH_4 on MgO-supported noble metals. The high reforming activity of Ru and Rh, compared to other transition metals, has been also confirmed by experimental measurements and first principle calculations, which showed that Ru and Rh are the most active pure transition metals for methane steam reforming, while Ni, Ir, Pt, and Pd are significantly less active at similar dispersion [66].

Regarding selectivity to reaction products, results obtained over the four most active Al_2O_3-supported catalysts (10%Ni, Ru, Rh, and Ir) are shown in Fig. 5B and C. It is observed that selectivity toward H_2 is higher than 90% for all four catalysts in the whole temperature range investigated and exceeds 97% at 750 °C, where $X_{C3H8} \approx 100\%$. The only hydrogen-containing byproduct detected over these catalysts is CH_4, the formation of which is favored at intermediate temperatures (Fig. 5B). Selectivity toward CH_4 at temperatures lower than *ca.* 600 °C is higher for the most active 10%Ni and Ru catalysts, compared to Rh and Ir, which can be attributed to the high activity of the former metals for the CO/CO_2 methanation reactions ([67] and refs therein). Qualitatively similar results have been reported by Kokka et al. [33] who studied the propane SR reaction over supported metals and found that methane selectivity at low temperatures is higher for the most active catalysts and that the temperature at which the maximum CH_4 selectivity appears shifts toward higher temperatures with decreasing catalytic activity. It should be noted that the production of C_2H_4, originating from the decomposition of propane ($C_3H_8 \rightarrow C_2H_4 + CH_4$), was detected in appreciable amounts only over the less-active Pd/Al_2O_3 and Re/Al_2O_3 catalysts at temperatures higher than *ca.* 600 °C (Supplementary Information, Fig. S2). Selectivities toward CO_2 and CO are practically the same for Ni, Ru, and Ir catalysts whereas Rh is more selective toward CO (Fig. 5C). This is in general agreement with results reported by Kolb et al. [23], who found that Rh was more active than Pt and Pd catalysts for the propane SR and exhibited higher selectivity ratios of CO/CO_2.

Summarizing, results presented in Fig. 5 show that Al_2O_3-supported Ru and Rh catalysts combine high propane conversions and high selectivities toward H_2 at temperatures above 650 °C, which are comparable to those of the reference $10\%Ni/Al_2O_3$ catalyst. It should be noted, however, that the metal loading is much higher for the latter sample.

3.2.2. *Effects of the nature of the support*

The choice of the support is known to affect the activity, product distribution, and stability of dispersed metal catalysts for steam reforming reactions [20,30,33,37,44], mainly because it participates in

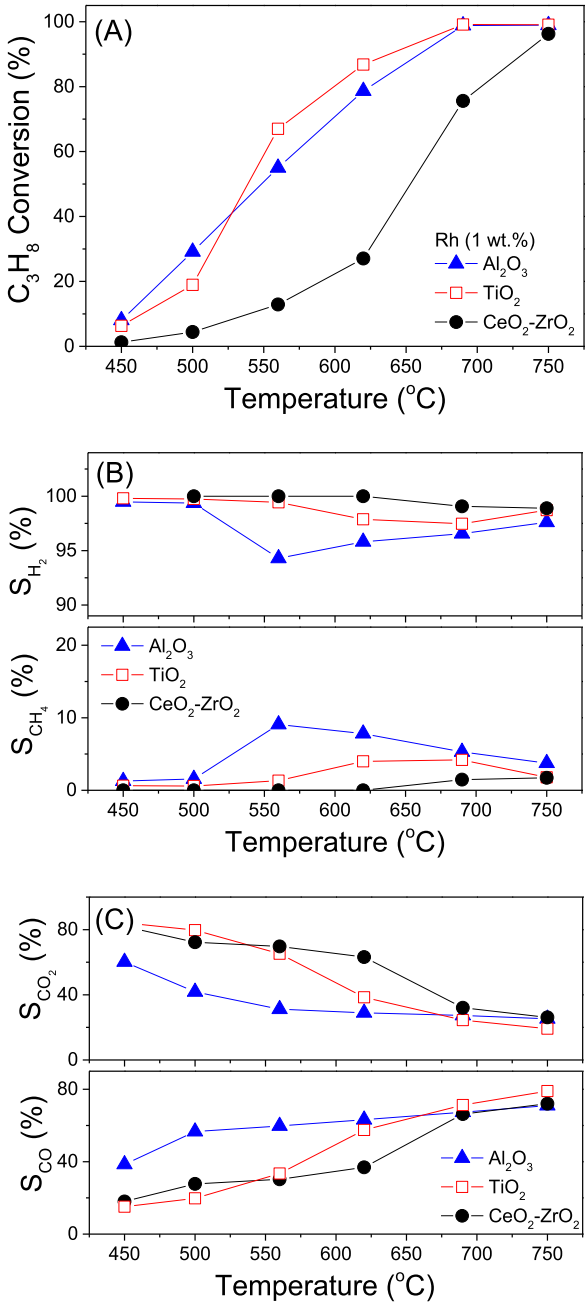

Fig. 6. (A) Conversion of propane, (B) selectivities to H_2 and CH_4, and (C) selectivities to CO_2 and CO obtained over Rh (1 wt%) catalysts dispersed on the indicated supports. Experimental conditions: same as in Fig. 4.

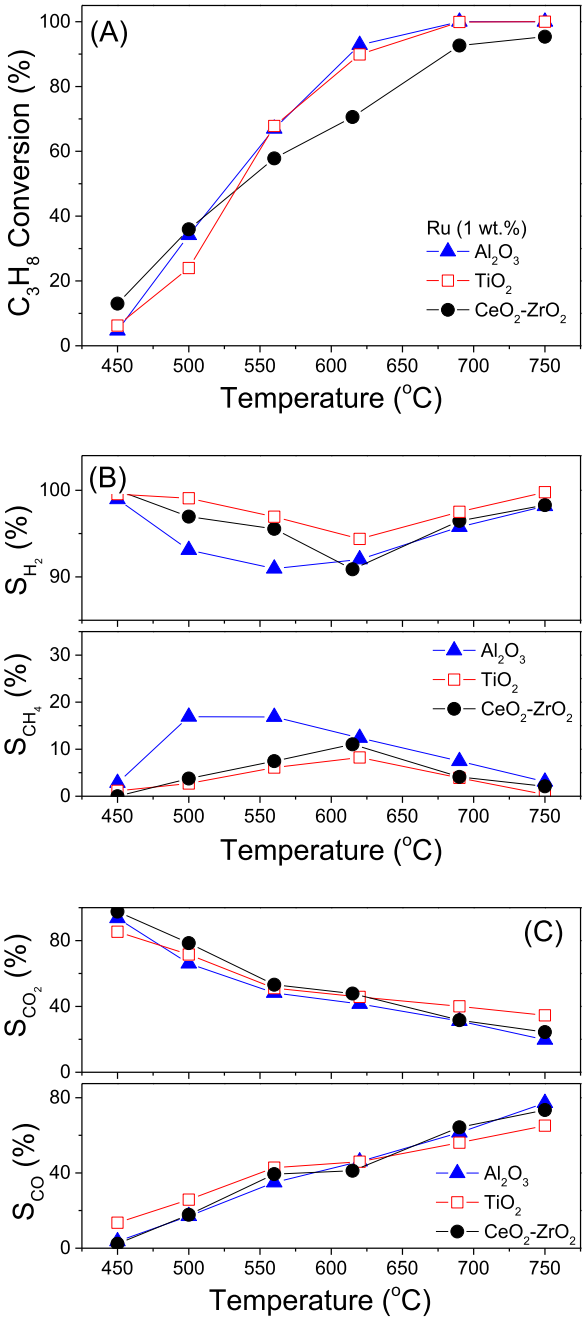

Fig. 7. (A) Conversion of propane, (B) selectivities to H_2 and CH_4, and (C) selectivities to CO_2 and CO obtained over Ru catalysts (1 wt%) dispersed on the indicated supports. Experimental conditions: same as in Fig. 4.

the water activation steps [23,32]. In this respect, the effects of the nature of the supporting material on catalytic performance have been examined over the best-performing Rh and Ru catalysts (1 wt%) dispersed on commercial Al_2O_3, TiO_2 or CeO_2-ZrO_2. Regarding the Rh catalysts (Fig. 6), it is observed that the propane conversion curves are comparable for Rh/Al_2O_3 and Rh/TiO_2 with X_{C3H8} being somewhat higher for the latter sample at temperatures above 550 °C (Fig. 6A). On the other hand, the Rh/CeO_2-ZrO_2 catalyst is much less active, which is evidenced by the shift of the propane conversion curve toward significantly higher temperatures. The high activity of Rh/TiO_2 for propane steam reforming has been reported by Yu et al. [31] and was attributed to the existence of metal-support interactions. The same group compared $Rh/Ce_{1-x}Zr_xO_2$ catalysts with Rh/γ-Al_2O_3 and reported that $Rh/Ce_{0.25}Zr_{0.75}O_2$ exhibited the highest activity [32]. Qualitatively similar results have been reported by Alphonse et al. [44] who found that the catalytic activity for propane SR over titania- and ceria-zirconia-supported metals was considerably higher than that of alumina-based catalysts. The comparably lower activity observed in the present work for the Rh/CeO_2-ZrO_2 catalyst (Fig. 6A) can be attributed to the different composition of the commercial CeO_2-ZrO_2 support employed here (13%Ce, balance Zr+Hf, according to the manufacturer) compared to that used in the above studies ($Ce_{0.25}Zr_{0.75}O_2$ in [32]; $Ce_{0.5}Zr_{0.5}O_2$ in [44]). Regarding selectivity, the only products detected for the three Rh catalysts investigated were H_2, CO, CO_2, and CH_4. The Rh/CeO_2-ZrO_2 catalyst is highly selective toward H_2 (S_{H2} > 98%) followed by Rh/TiO_2 (Fig. 6B). The Rh/Al_2O_3 sample exhibits comparably higher selectivity toward methane in the whole temperature range investigated with S_{CH4} reaching a maximum of *ca.* 10% at 560 °C. This

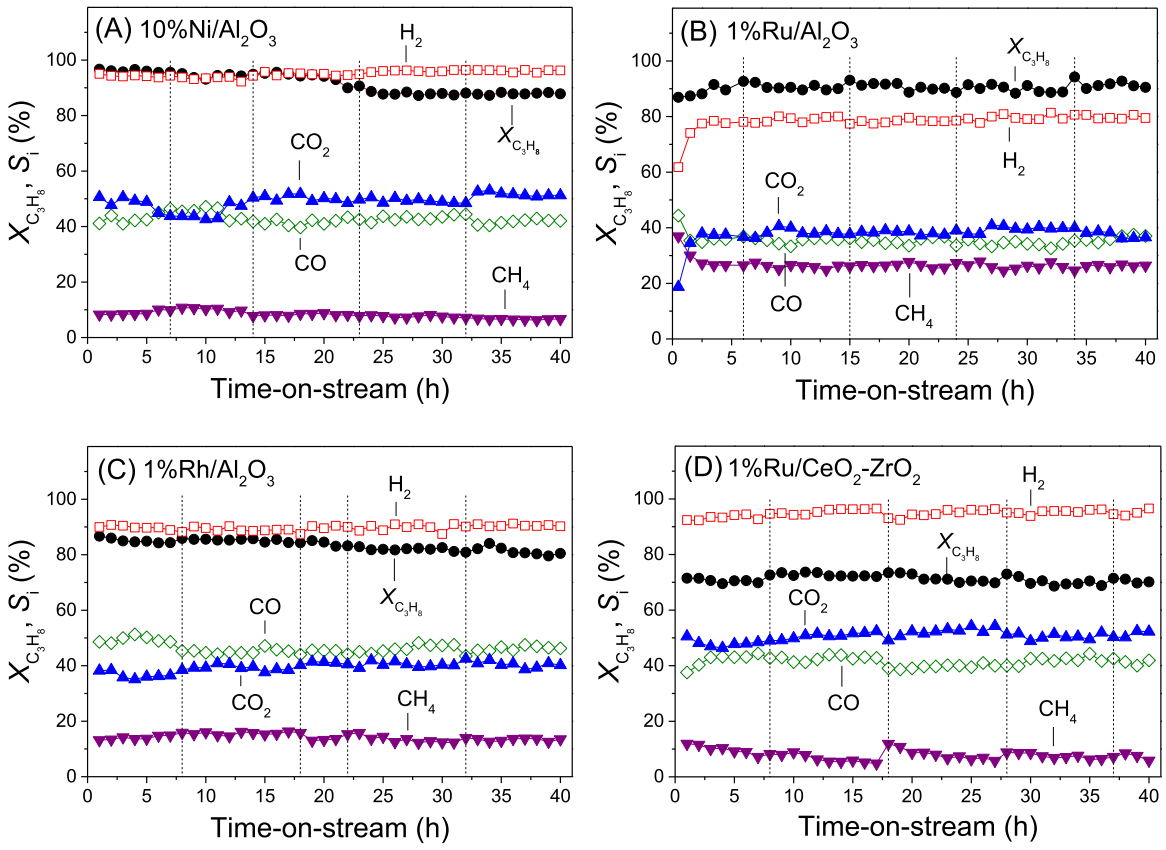

Fig. 8. Results of long-term stability tests obtained under propane steam reforming reaction conditions at $T = 600$ °C for (A) 10%Ni/Al_2O_3, (B) 1%Ru/Al_2O_3, (C) 1% Rh/Al_2O_3 and (D) 1%Ru/CeO_2-ZrO_2 catalysts. Experimental conditions: same as in Fig. 4. Vertical lines indicate shutting down of the system overnight, where the catalyst was kept at room temperature under He flow.

can be related, at least in part, to the higher dispersion of Rh on Al_2O_3, compared to TiO_2 and CeO_2-ZrO_2 (Table 1), since the structure sensitive CO and CO_2 hydrogenation reactions are generally favored with decreasing particle size, at least for small metal crystallites [33,68]. However, at higher temperatures, S_{H2} exceeds 95% for all three Rh catalysts studied. As shown in Fig. 6C, the Rh/TiO_2 and Rh/CeO_2-ZrO_2 catalysts exhibit higher selectivities toward CO_2, compared to Rh/Al_2O_3, which decreases with the increase of temperature due to the occurrence of the RWGS reaction.

Similar experiments were performed over Ru catalysts and the results obtained are summarized in Fig. 7. It is observed that the propane conversion curves are not much different for the three samples, although X_{C3H8} takes lower values over the Ru/CeO_2-ZrO_2 catalyst at temperatures higher than *ca.* 550 °C (Fig. 7A). The Ru/TiO_2 and Ru/CeO_2-ZrO_2 catalysts exhibit higher selectivities towards H_2 at temperatures lower than *ca.* 500 °C while the Al_2O_3-supported sample produces larger amounts of CH_4 (Fig. 7B) as was also observed for the Rh/Al_2O_3 catalyst discussed above. Regarding selectivities toward CO_2 and CO, they are practically the same for the three Ru catalysts in the whole temperature range investigated (Fig. 7C).

3.2.3. Catalyst stability

Results presented above show that Rh and Ru exhibit the highest propane conversion, compared to the rest of Al_2O_3-supported metal catalysts investigated (Fig. 5), whereas Ru/CeO_2-ZrO_2 (Fig. 7) is considerably more active compared to Rh/CeO_2-ZrO_2 (Fig. 6). In this respect, the 1%Rh/Al_2O_3, 1%Ru/Al_2O_3, and 1%Ru/CeO_2-ZrO_2 catalysts were selected to study their stability under reaction conditions, compared to the reference 10%Ni/Al_2O_3 sample. It may be noted that TiO_2-supported catalysts were not further investigated because of the significant decrease of their specific surface area at high temperatures (Table 1).

Results obtained following exposure of the selected catalysts to propane SR reaction conditions at 600 °C for 40 h are presented in Fig. 8, where X_{C3H8} and selectivities toward H_2, CH_4, CO, CO_2 are plotted as functions of time-on-stream. In these graphs, vertical lines indicate shutting down of the system overnight, where the catalyst was kept at room temperature under He flow. It is observed that the reference 10%Ni/Al_2O_3 catalyst exhibits the highest initial propane conversion (97%), which drops to *ca.* 88% after 25 h-on-stream and does not change appreciably until the end of the run (Fig. 8A). Selectivities to reaction products are generally stable with time with S_{H2} remaining practically constant at *ca.* 96%.

The Ru/Al_2O_3 catalyst (Fig. 8B) exhibits a very stable performance, with propane conversion acquiring values of *ca.* 92%, *i.e.* higher than that obtained for the 10%Ni catalyst after 40 h-on-stream. However, S_{H2} is considerably lower, compared to 10%Ni, taking values around 80%. The Rh/Al_2O_3 catalyst (Fig. 8C) is characterized by a higher H_2-selectivity (91%), compared to Ru/Al_2O_3, but is less stable as indicated by the progressive and continuous decrease of X_{C3H8} from 86% to 81% with time-on-stream. Finally, the Ru/CeO_2-ZrO_2 catalyst (Fig. 8D) is very stable and selective toward H_2 (S_{H2}=96%) but is characterized by relatively low propane conversion (*ca.* 70%), compared to the Al_2O_3-supported Rh and Ru catalysts.

Summarizing, results presented in Fig. 8 show that the two Ru catalysts, namely Ru/Al_2O_3 and Ru/CeO_2-ZrO_2, are characterized by higher stability with time-on-stream for the propane steam reforming reaction at 600 °C, compared to Rh/Al_2O_3 and 10%Ni/Al_2O_3. In addition, the Ru/CeO_2-ZrO_2 catalyst, although less active, exhibits the highest selectivity toward H_2 (> 95%).

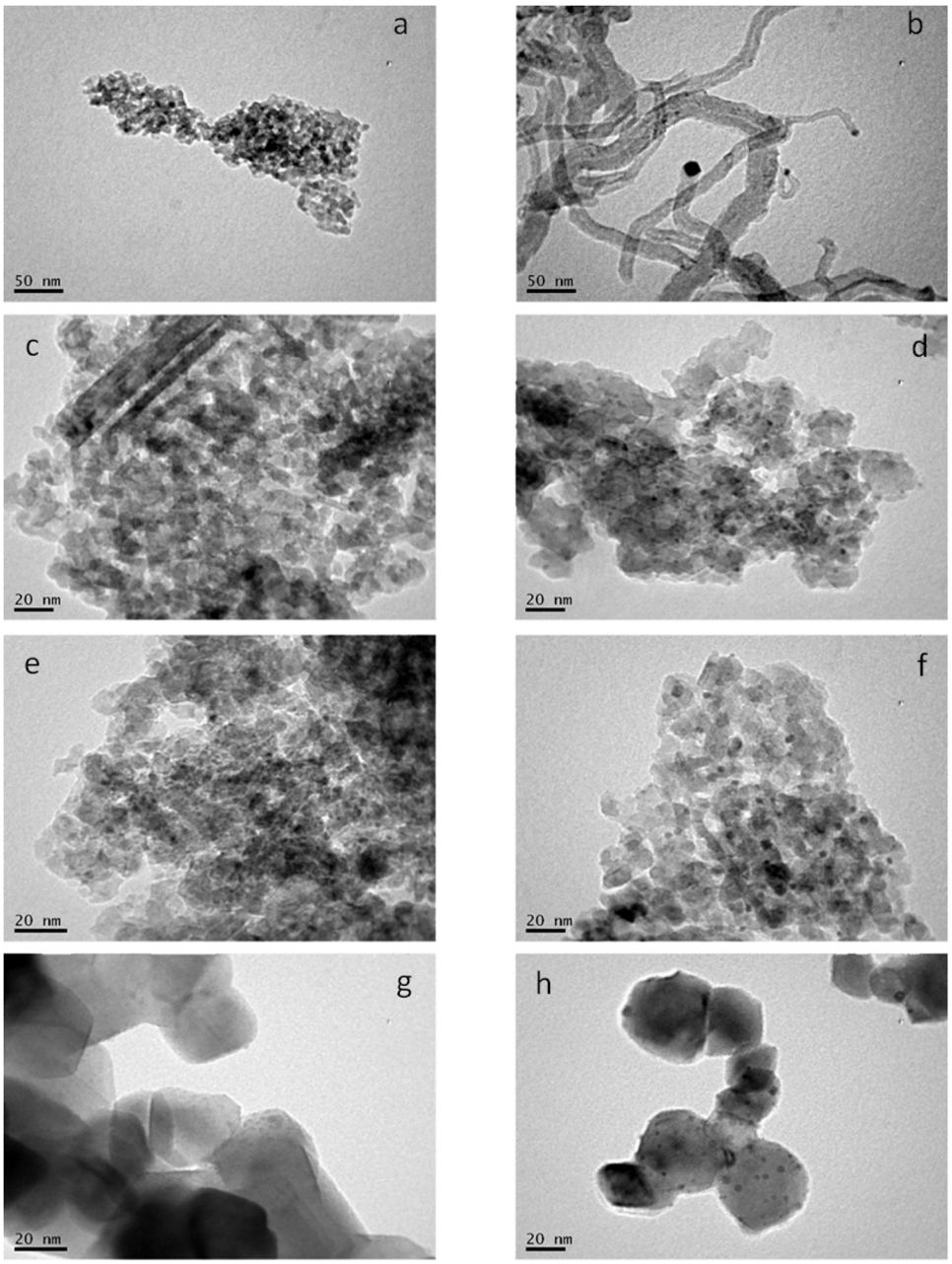

Fig. 9. Representative TEM images of the fresh (left) and used (right) Ni/Al_2O_3 (a, b), Rh/Al_2O_3 (c, d), Ru/Al_2O_3 (e, f) and Ru/CeO_2-ZrO_2 (g, h) catalyst samples.

3.2.4. *Microstructure of fresh and used catalysts*

In Fig. 9 are shown representative TEM images obtained for the 10% Ni/Al_2O_3, Rh/Al_2O_3, Ru/Al_2O_3 and Ru/CeO_2-ZrO_2 catalysts before and after the stability tests presented in Fig. 8. It is observed that, in all cases, the metal particles are well dispersed on the catalyst surfaces. The size distribution of the dispersed metal crystallites was determined for each sample by measuring at least 100 randomly selected nanoparticles in the respective TEM images. Results obtained are summarized in Fig. 10, and the calculated average metal crystallite sizes are listed in Table 2. It is observed that the as prepared $10\%Ni/Al_2O_3$ catalyst is characterized by the presence of relatively large crystallites, which is due to the high Ni loading. Exposure to reaction conditions for 40 h results in a substantial increase of the mean particle size from *ca.* 5.6–21 nm (Table 2), which is due to the sintering of the Ni particles induced by the application of high reforming temperatures and the presence of steam [2]. Regarding the three noble metal catalysts, the mean metal crystallite size of the fresh samples is typically less than 2 nm but also increases following exposure to reaction conditions (Fig. 10, Table 2). This increase is more pronounced for the Ru/Al_2O_3 and Ru/CeO_2-ZrO_2 catalysts, compared to Rh/Al_2O_3, indicating the higher tendency of Ru toward sintering under the present reaction conditions.

3.2.5. *Carbon accumulation*

It is well documented that the deactivation of catalytic materials under SR reaction conditions is mainly due to carbon accumulation on the catalyst surface [43]. Thermodynamic analyses predict that carbon formation during steam reforming and oxidative steam reforming of propane and butane is favored at low steam-to-carbon ratios ($S/C < 2$) and temperatures in the range 550–650 °C [69]. Carbon deposition occurs, mainly, *via* decomposition of reactant (Eq. (10)) and byproduct hydrocarbons, such as CH_4 (Eq. (11)), the Boudouard reaction (Eq. (12)), and the CO hydrogenation reaction (Eq. (13)) [37,43,70]:

$$C_nH_{2n+2} \rightarrow (n+1)H_2 + nC \quad (10)$$

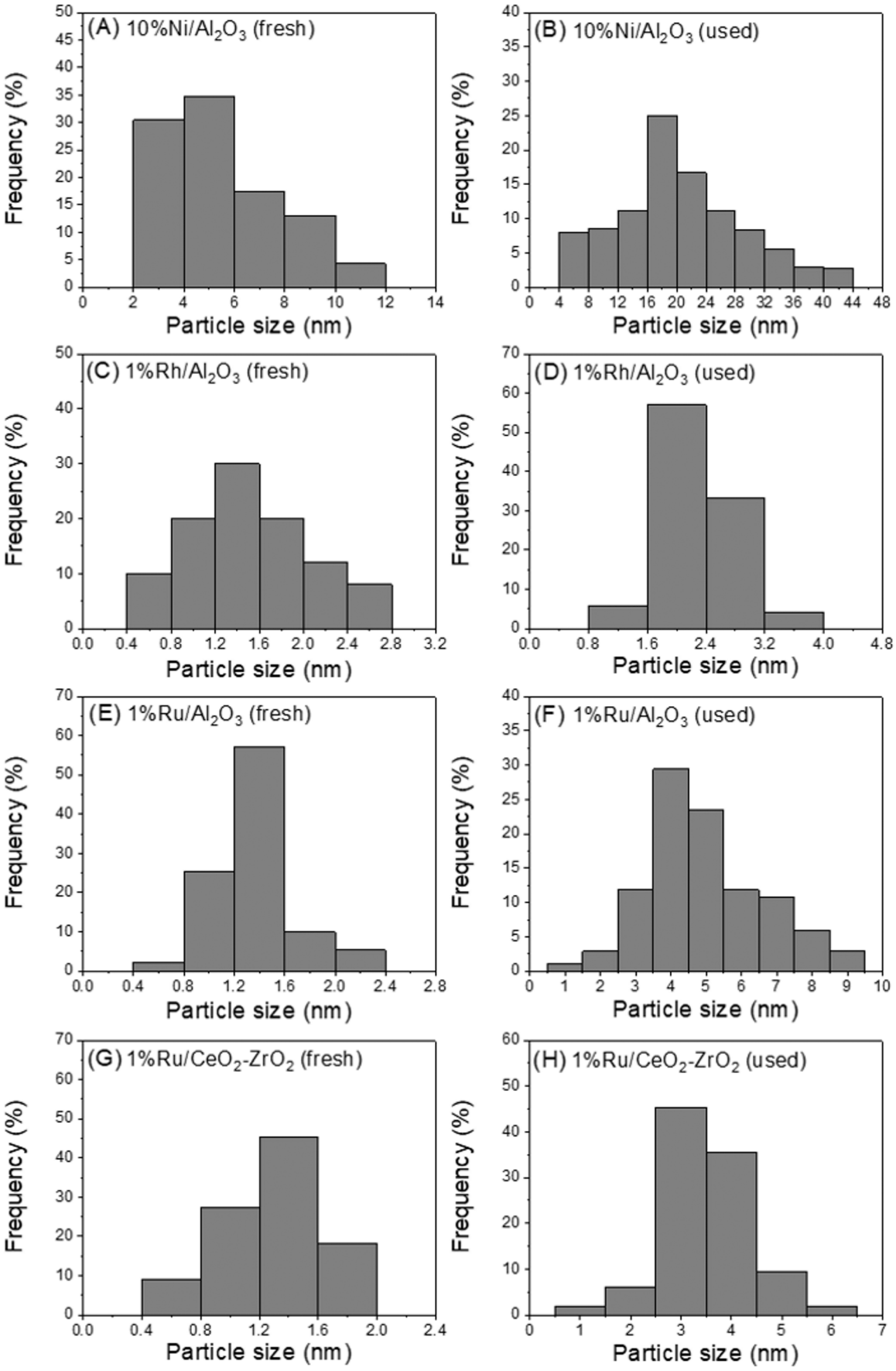

Fig. 10. Particle size distribution of the indicated fresh (left) and used (right) catalysts.

Table 2
Mean metal crystallite sizes determined from the TEM images of the indicated catalysts obtained before and after exposure to the stability tests presented in Fig. 8.

Catalyst	Mean metal crystallite size (nm)	
	Fresh	Used
10%Ni/Al_2O_3	5.6	21
Rh/Al_2O_3	1.7	2.3
Ru/Al_2O_3	1.3	5.0
Ru/CeO_2-ZrO_2	1.4	3.6

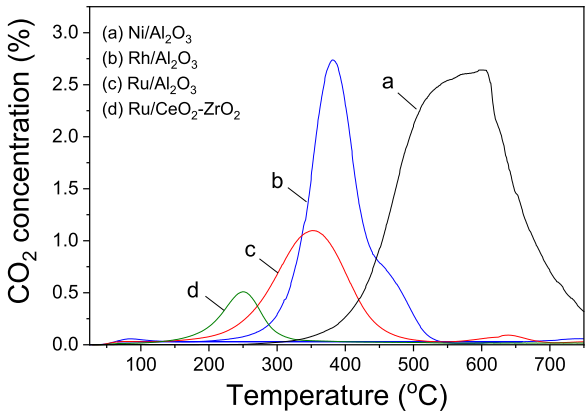

Fig. 11. Temperature-programmed oxidation (TPO) profiles obtained over the indicated catalysts following exposure to the long-term stability tests shown in Fig. 8.

$$CH_4 \leftrightarrow 2H_2 + C \quad (11)$$

$$2CO \leftrightarrow CO_2 + C \quad (12)$$

$$CO + H_2 \leftrightarrow H_2O + C \quad (13)$$

Reactions (12) and (13) are favored at lower temperatures and can be suppressed using high S/C ratios whereas reactions (10) and (11) become increasingly important at higher temperatures [37,70]. Considering the relatively high S/C ratios used in the present study and the reaction temperature employed (600 °C) for the stability tests (Fig. 8), carbon formation should be mainly attributed to the decomposition of hydrocarbons on the catalyst surfaces according to reactions (10) and (11).

Quantification of the carbon species deposited on the catalyst surfaces following the long-term stability tests (Fig. 8) was accomplished with TPO experiments and results obtained are summarized in Fig. 11, where the CO_2 concentration at the reactor effluent is plotted as a function of temperature. It is observed that the TPO profile of the 10% Ni/Al_2O_3 catalyst is characterized by the presence of an intense CO_2 peak with a broad maximum located at *ca.* 500–600 °C (trace a). The amount of accumulated carbon, calculated from the area below the TPO curve, is relatively high (56 mg C g_{cat}^{-1}) and may explain the decrease of propane conversion observed for this catalyst after *ca.* 20 h-on-stream (Fig. 8A). It is believed that the accumulation of carbon on Ni-based catalysts involves dissociation of the hydrocarbon on the catalyst surface, which leads to the formation of monoatomic carbon (C_α) [70]. This species is highly reactive and can be easily gasified under reaction conditions. However, if the gasification rate is slow, C_α can be polymerized to a much less reactive carbon type (C_β). Due to the slower gasification rate of C_β, this species may accumulate on the catalyst surface and/or dissolve in the metal resulting in the formation of vermicular carbon (C_V), which can further form carbon fibers and whiskers [37,70]. Results of previous studies performed over Ni/Al_2O_3 catalysts showed that the TPO profiles recorded after propane SR reactions are characterized by two peaks located at *ca.* 360 °C and 640 °C, attributable to monoatomic carbon and filamentous carbon, respectively [25]. Based on its position, the CO_2 peak observed in this work for the 10%Ni/Al_2O_3 catalyst (trace a) can be attributed to filamentous and/or graphitic carbon, the gasification of which is known to take place in the temperature range 500–800 °C [71]. The presence carbon filaments on the surface of the Ni/Al_2O_3 catalyst is clearly evidenced from the TEM image obtained for this sample following exposure to reaction conditions (Fig. 9b).

The TPO profile of the Rh/Al_2O_3 catalyst is characterized by an intense peak centered at 385 °C and a high-temperature shoulder located at *ca.* 460 °C (trace b). As discussed above, the peak at 385 °C can be attributed to monoatomic carbon (C_α) formed by the dehydrogenation of hydrocarbon fragments on the catalyst surface [37], which can be easily gasified by H_2O and/or H_2 under SR conditions [25], whereas the shoulder at 460 °C can be assigned to polymeric amorphous carbon (C_β), which is produced from C_α when this is not removed at sufficiently high rates from the catalyst surface [37]. It is of interest to note that the amount of carbon accumulated on the Rh/Al_2O_3 catalyst (43 mg C g_{cat}^{-1}) is much lower than that on 10%/Ni/Al_2O_3 (56 mg C g_{cat}^{-1}) and is oxidized at much lower temperatures during TPO.

The TPO profile of Ru/Al_2O_3 catalyst consists of a relatively less intense CO_2 peak centered at *ca.* 350 °C (trace c), which is attributable to C_α species. The amount of accumulated carbon (26 mg C g_{cat}^{-1}) is considerably lower than that obtained for the 10%Ni and Rh catalysts dispersed on the same support (compare with traces a and b, respectively) indicating that Ru has a lower tendency toward carbon accumulation, compared to the other two metals. This can be explained considering that carbon formation over ruthenium (and also rhodium) catalysts occurs *via* a different mechanism, compared to nickel, and because Ru (and also Rh) cannot dissolve carbon to the same extent as Ni [43]. Similar TPO peaks located in the range 340–390 °C have been reported by Rezaei et al. [72] for Ru, Rh, Ir, Pt, and Pd catalysts supported on alumina-stabilized magnesia under CO_2 reforming of methane and were assigned to oxidation of amorphous carbon. The higher activity of Ru and Rh, compared to other catalysts, was correlated to the formation of the highly reactive C_α species [72].

Finally, the Ru/CeO_2-ZrO_2 catalyst presents a very small TPO peak located at 250 °C (trace d), which corresponds to only 7 mg C g_{cat}^{-1}. It should be noted, however, that this sample was the least active among the four catalysts investigated in this set of experiments (Fig. 8). The CO_2 peak observed at 250 °C appears at a temperature similar to that reported by Hou et al. (236 °C) [29] who studied propane SR over an Ir/$Ce_{0.75}Zr_{0.25}O_2$ catalyst at 600 °C and found that it exhibited a stable catalytic performance for 65 h-on-stream without obvious deactivation. It is believed that TPO peaks appearing at such low temperatures are due to reactive carbon deposits located near the metallic particles, which can be more easily oxidized, especially in the presence of reducible supports [73]. It is known that the presence of rare earth oxides on the support significantly decreases carbon accumulation under SR reaction conditions by enhancing coke gasification and, consequently, the catalyst surface is kept free of coke [43]. In the case of CeO_2-containing catalysts, it is believed that the reducible oxide transports oxygen to the dispersed metal, thereby promoting gasification of carbon deposits, and is then reoxidised by H_2O (or CO_2) [23,25,36]. This reasoning may explain the high stability of the present Ru/CeO_2-ZrO_2 catalyst with time-on-stream (Fig. 8D) and indicates that the rate of carbon deposition over this sample is lower than the rate of oxygen transfer from the support and the subsequent carbon oxidation. In this respect, the observed resistance of the Ru/CeO_2-ZrO_2 catalyst against carbon accumulation can be attributed to the redox properties of the CeO_2-ZrO_2 support and the availability of highly labile lattice oxygen species under SR reaction conditions.

It should be noted that the amount of accumulated on the catalyst

Table 3
Amount of carbon accumulated on the catalyst surfaces per mol of converted hydrocarbon (HC) during the long-term-stability tests.

Catalyst sample	Amount of accumulated carbon, mg C (mol HC)$^{-1}$ g_{cat}^{-1}	
	Propane SR at 600 °C	LPG SR at 550 °C
Ni/Al_2O_3	122	–
Rh/Al_2O_3	101	32
Ru/Al_2O_3	56	26
Ru/CeO_2-ZrO_2	19	2

surfaces during the stability tests presented in Fig. 8 also depends on propane conversion. In order to take into account this parameter, the amount of accumulated carbon per mole of converted propane was calculated and results obtained are presented in Table 3. It is observed that the values obtained follow the order $Ni/Al_2O_3 > Rh/Al_2O_3 > Ru/Al_2O_3 > Ru/CeO_2$-$ZrO_2$. This verifies the resistance of the Ru/CeO_2-ZrO_2 catalyst against carbon deposition and explains its high stability under propane SR conditions.

Summarizing, the results of stability tests (Fig. 8) and subsequent TPO experiments (Fig. 11) performed over the three Al_2O_3-supported samples show that the 10%Ni/Al_2O_3 and Rh/Al_2O_3 catalysts are not very stable under the propane SR reaction conditions employed due to the accumulation of inactive carbon on their surface, which is much more important for the 10%Ni sample. In contrast, Ru/Al_2O_3 exhibits a stable performance (Fig. 8B) and is characterized by the accumulation of much lower amounts of carbon, which can be oxidized at relatively low temperatures (<450 °C). The Ru/CeO_2-ZrO_2 catalyst, although less active than the above three Al_2O_3-supported catalysts, exhibits very good stability with time-on-stream (Fig. 8D), which can be related to its ability to accumulate very small amounts of easily oxidizable carbon (< 300 °C) on its surface (Fig. 11).

3.3. Steam reforming of LPG using concentrated feeds

As discussed above, LPG can be represented by a mixture of propane and butane [22]. In this respect, the three precious metal catalysts, which exhibited the best performance in terms of propane conversion, hydrogen selectivity and long-term stability (Rh/Al_2O_3, Ru/Al_2O_3 and Ru/CeO_2-ZrO_2), were further investigated to study the effects of the presence of butane in the feed. It should be noted that this set of experiments was performed using a concentrated feed consisting of 7.1% LPG ($C_3H_8 + C_4H_{10}$) and 68% H_2O, compared to 2.3% C_3H_8 and 22.9% H_2O used in the experiments presented in Section 3.2. In addition, the stability tests were performed at a lower temperature (550 °C), compared to that used in Section 3.2 (600 °C).

3.3.1. Rh/Al_2O_3 catalyst

In Fig. 12 are summarized results of catalytic performance tests obtained over the Rh/Al_2O_3 catalyst with the use of three different propane:butane molar ratios in the feed (100:0, 95:5, 85:15). It may first be noted that the propane conversion curve recorded in the absence of butane in the feed (100:0 mixture) is shifted toward slightly higher temperatures (Fig. 12A), compared to that obtained with the use of the diluted feed under otherwise the same conditions (see Fig. 5A). Replacement of 5% of propane with butane (95:5 mixture) results in a shift of the X_{C3H8}-curve toward higher temperatures by *ca.* 50 °C, compared to the 100:0 mixture, which becomes even more significant upon further increasing the butane content (85:15 mixture) (Fig. 12A). This behavior can be explained considering that butane adsorbs more strongly than propane on the catalyst surface thereby inhibiting the conversion of the latter. Comparison of results presented in Fig. 12A and

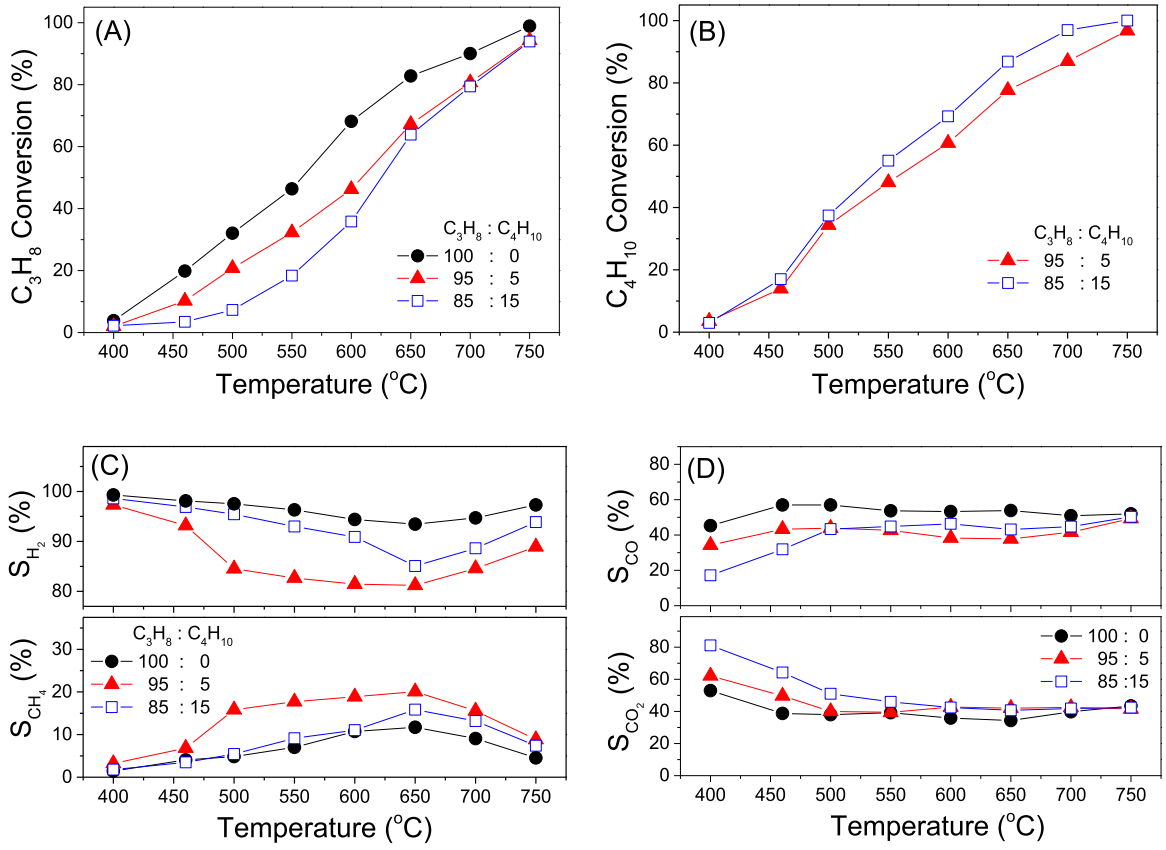

Fig. 12. Effects of inlet gas composition (C_3H_8:C_4H_{10} molar ratio) on the catalytic performance of the 1%Rh/Al_2O_3 catalyst: (A) C_3H_8 conversion; (B) C_4H_{10} conversion; (C) selectivities to H_2 and CH_4; (D) selectivities to CO_2 and CO. Feed composition: 7.1% (C_3H_8 +C_4H_{10}) and 68% H_2O (balance He); total flow rate (*F*): 270 cm^3 min^{-1}; other experimental conditions same as in Fig. 4.

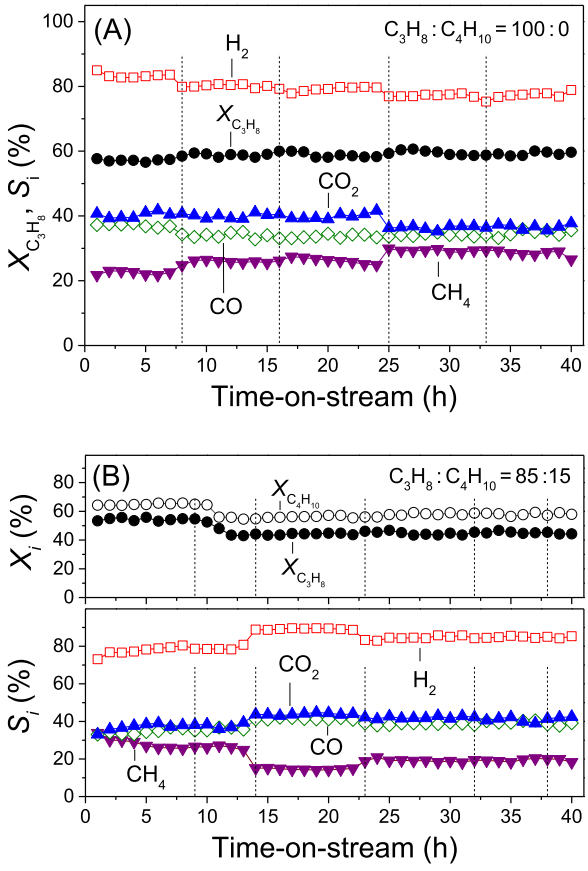

Fig. 13. Performance with time-on-stream of the 1%Rh/Al_2O_3 catalyst at $T = 550$ °C (A) in the absence of butane (100:0 mixture) and (B) in the presence of butane (85:15 mixture) in the feed. Other experimental conditions same as in Fig. 12.

B shows that, for both the 95:5 and 85:15 mixtures, the conversion of butane at a given temperature is always higher than that of propane. This is in agreement with the general trend that the reactivity of hydrocarbons increases with increasing the size of the molecule [72]. Selectivity toward H_2 decreases substantially upon replacing 5% of propane with butane (95:5 mixture), which is accompanied by an increase of S_{CH4} (Fig. 12C). However, further increase of the butane content (85:15 mixture) results in an increase of S_{H2} at the expense of S_{CH4}. This reveals the complexity of the reactions that take place during the LPG reforming process and imply that the prediction of the catalytic performance is not always possible and requires experimental verification. Regarding the selectivity toward CO_2, it generally increases with increasing the butane content in the feed (Fig. 12D). However, the S_{CO2} and S_{CO} curves are not significantly different at temperatures higher than *ca.* 500 °C.

The long-term stability of the 1%Rh/Al_2O_3 catalyst was investigated at 550 °C with the use of concentrated feeds and results obtained in the absence and the presence of butane are shown in Fig. 13. Regarding the 100:0 mixture, it is observed that X_{C3H8} remains stable throughout the experiment, taking values close to 60% (Fig. 13A). However, S_{H2} decreases progressively with time-on-stream from an initial value of 85–77% after 40 h. Selectivity toward methane follows an opposite behavior with S_{CH4} increasing from 23% to *ca.* 29% with time-on-stream. Moreover, both S_{CO2} and S_{CO} progressively decrease with time. This variation of selectivities to reaction products indicates that the performance of the 1%Rh/Al_2O_3 catalyst deteriorates with time-on-stream under these conditions.

Replacement of 15% of propane by butane in the feed (85:15 mixture) results in initial conversions of $X_{C3H8} = 55\%$ and $X_{C4H10} = 65\%$

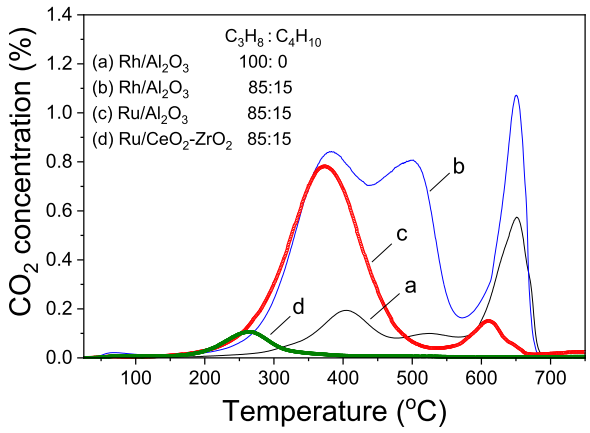

Fig. 14. Temperature-programmed oxidation (TPO) profiles obtained for the indicated catalysts and C_3H_8:C_4H_{10} ratios in the feed following the long-term stability tests shown in Fig. 13 (traces a and b), Fig. 16 (trace c) and Fig. 18 (trace d).

(Fig. 13B). These values drop to *ca.* 45% and 56%, respectively, after about 12 h-on-stream and then remain practically constant until the end of the experiment. Selectivity toward H_2 increases progressively from 77% to 85%, at the expense of S_{CH4} while S_{CO2} and S_{CO} do not vary appreciably, especially after more than *ca.* 14 h-on-stream.

Results of TPO experiments performed after the above stability tests are shown in Fig. 14. It is observed that the TPO profile obtained following exposure of the Rh catalyst to the 100:0 mixture is characterized by the presence of three peaks located at *ca.* 400 °C, 525 °C, and 650 °C (trace a). The first two peaks appear at temperatures similar to those observed for this catalyst following exposure to the diluted 100:0 mixture at 600 °C (Fig. 11) and, as discussed above, can be assigned to monoatomic carbon (C_α) and polymeric amorphous carbon (C_β), respectively. The third peak located at 650 °C, which is of much higher relative intensity, can be attributed to graphitic carbon associated with the support. It is generally believed that TPO peaks appearing at such high temperatures originate from the oxidation of carbon deposited on the support whereas the low-temperature peaks are due to oxidation of carbon deposited in the vicinity of the metal particles [38,73]. The appearance of the 650 °C peak indicates that the present reaction conditions favor the accumulation of inactive carbon on the catalyst surface, which is not easily oxidized.

A qualitatively similar TPO profile was obtained following exposure of the Rh catalyst to the 85:15 mixture (trace b). However, all three peaks are of much higher intensity in this case and the amount of accumulated carbon (31 mg C g_{cat}^{-1}) is considerably higher, compared to that obtained with the 100:0 mixture (12 mg C g_{cat}^{-1}). Obviously, the presence of butane in the feed results in the accumulation of much higher amounts of carbon on the catalyst surface. This is in agreement with previous results showing that higher hydrocarbons have a greater tendency for carbon formation [74], and can be explained considering that dissociative adsorption is faster for higher hydrocarbons. Thus, although a similar sequence of reactions can be used to describe SR and carbon deposition reactions for propane and butane, the rate of carbon accumulation is expected to be faster and coking to be more pronounced in the presence of butane in the feed [70]. Results discussed above clearly show that evaluation of catalysts for the steam reforming of LPG cannot be based solely on experiments performed using only propane in the feed since carbon accumulation and catalytic performance depend strongly on the presence and concentration of butane in the reaction mixture.

3.3.2. *Ru/Al_2O_3 catalyst*

The steam reforming of LPG has been investigated over the 1%Ru/Al_2O_3 catalyst employing the same concentrated feeds used for the Rh/

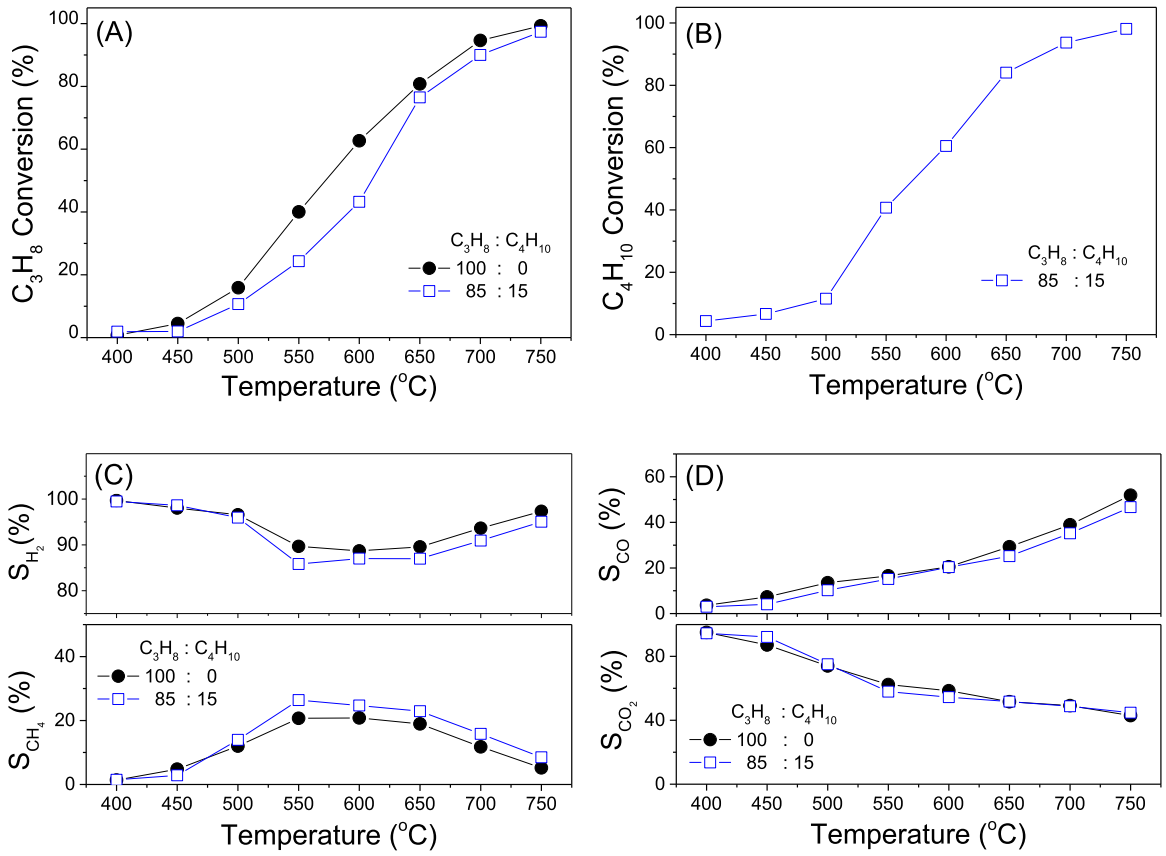

Fig. 15. Effects of inlet gas composition (C_3H_8:C_4H_{10} molar ratio) on the catalytic performance of the 1%Ru/Al_2O_3 catalyst: (A) C_3H_8 conversion; (B) C_4H_{10} conversion; (C) selectivities to H_2 and CH_4; (D) selectivities to CO_2 and CO. Experimental conditions same as in Fig. 12.

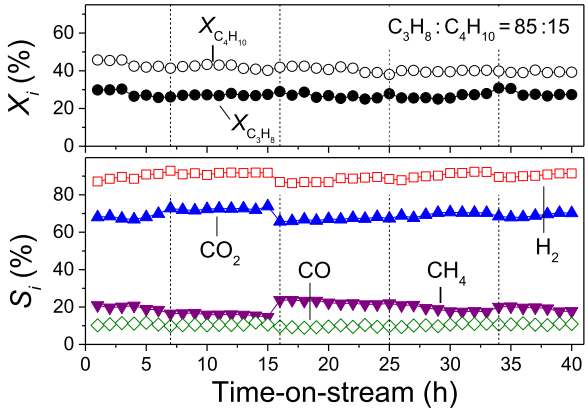

Fig. 16. Performance with time-on-stream of the 1%Ru/Al_2O_3 catalyst at $T = 550$ °C in the presence of butane (85:15 mixture) in the feed. Other experimental conditions same as in Fig. 12.

Al_2O_3 catalyst discussed above and the results obtained are summarized in Fig. 15. It is observed that the addition of butane in the feed (85:15 mixture) results in a relatively small shift of the X_{C3H8}-conversion curve toward higher temperatures (Fig. 15A) and that conversion of butane at a given temperature is higher than that of propane (Fig. 15B). Comparison with results presented in Fig. 12 shows that selectivity toward H_2 decreases slightly in the presence of butane while S_{CH4} follows the opposite trend (Fig. 15C). Regarding the selectivities toward CO and CO_2, they are not affected, practically, by the presence of butane in the feed (Fig. 15D).

The stability of the Ru/Al_2O_3 catalyst was investigated at 550 °C using the 85:15 propane:butane mixture and the results obtained are shown in Fig. 16. It is observed that the initial conversions of propane (30%) and butane (45%) are lower than those obtained for the Rh/Al_2O_3 catalyst under the same conditions (compare with Fig. 13B). However, both X_{C3H8} and X_{C4H10} are relatively more stable and do not vary appreciably after 40 h-on-stream. Furthermore, selectivities toward H_2 (~ 90%) and CO_2 (~ 70%) are considerably higher than those obtained for the Rh/Al_2O_3 catalyst.

The TPO profile of the Ru catalyst obtained after the stability test is shown in Fig. 14 (trace c). It is observed that CO_2 evolution is characterized by two peaks, one centered at 375 °C and one at 610 °C, which is of much lower intensity. Comparison with the TPO profile obtained for the Rh catalyst under the same conditions (trace b) shows that the peak at 375 °C (C_α) appears at the same temperature and is of similar intensity for the two samples. However, the peak at 500 °C (C_β) is not discernible in the TPO profile of the Ru catalyst and the high-temperature peak at 610 °C is considerably smaller, compared to that of the Rh catalyst. Regarding the amount of accumulated carbon, it is significantly lower for Ru (16 mg C g_{cat}^{-1}), compared to Rh catalyst (31 mg C g_{cat}^{-1}). The absence of the (C_β) peak (trace c) indicates that, under the present reaction conditions, the residence time of the active surface carbon species over the Ru/Al_2O_3 catalyst is too short to allow its efficient transformation toward the more inactive carbon forms that lead to the appearance of TPO peaks at temperatures higher than *ca.* 450 °C. It may then be concluded that carbon accumulation is significantly suppressed over the Ru catalyst because of its ability to efficiently gasify active carbon deposits.

3.3.3. *Ru/CeO_2-ZrO_2 catalyst*

Results of catalytic performance tests obtained over the 1%Ru/CeO_2-ZrO_2 catalyst in the absence and the presence of butane in the feed

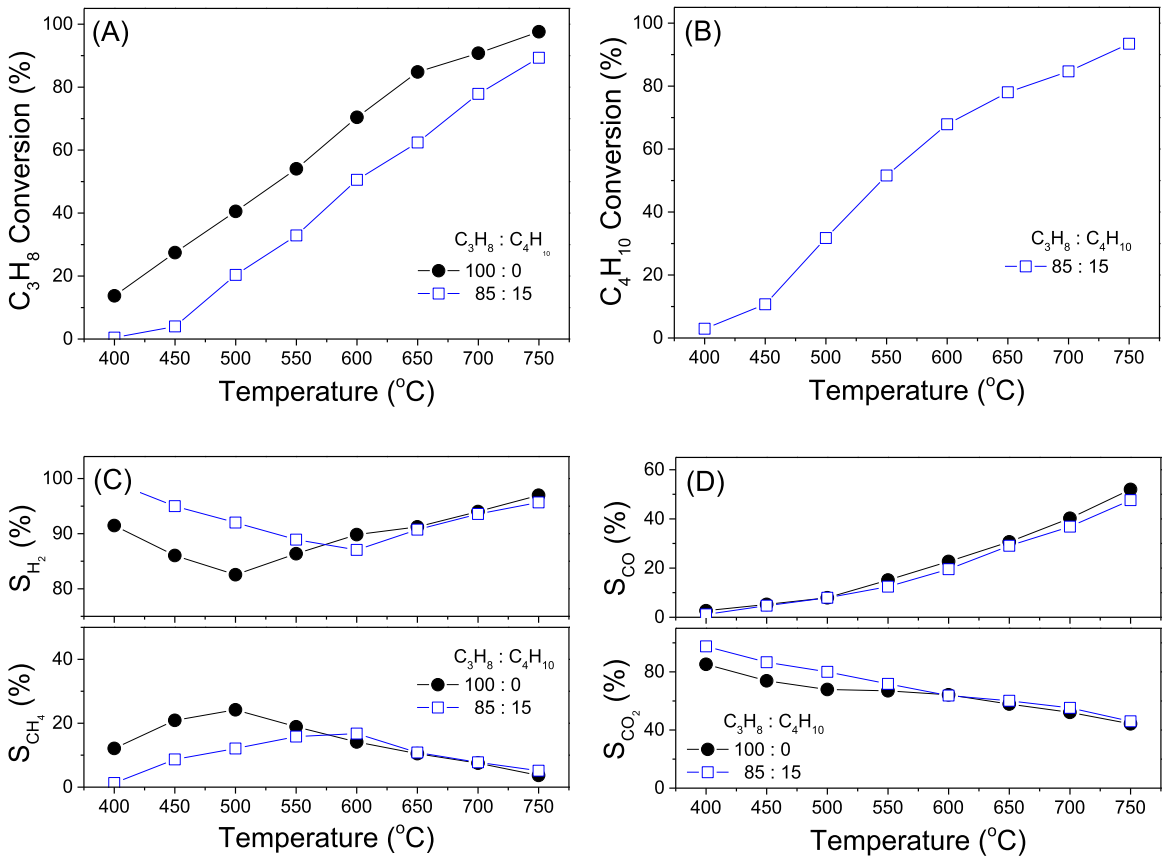

Fig. 17. Effects of inlet gas composition (C_3H_8:C_4H_{10} molar ratio) on the catalytic performance of the 1%Ru/CeO_2-ZrO_2 catalyst: (A) C_3H_8 conversion; (B) C_4H_{10} conversion; (C) selectivities to H_2 and CH_4; (D) selectivities to CO_2 and CO. Experimental conditions same as in Fig. 12.

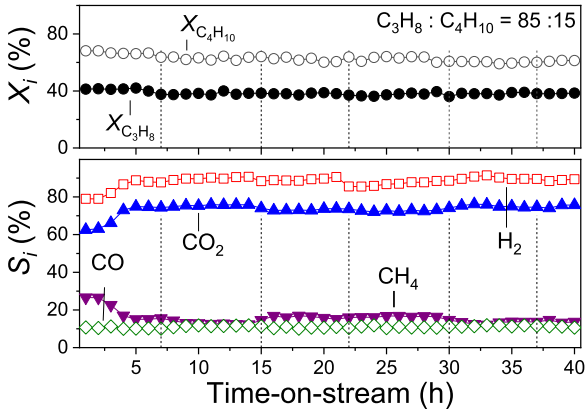

Fig. 18. Performance with time-on-stream of the 1%Ru/CeO_2-ZrO_2 catalyst at $T = 550$ °C in the presence of butane (85:15 mixture) in the feed. Other experimental conditions same as in Fig. 12.

(85:15 mixture) are summarized in Fig. 17. It is observed that the addition of butane results in a significant shift of the propane conversion curve toward higher temperatures (Fig. 17A) and that the catalyst promotes more efficiently the conversion of butane (Fig. 17B). Interestingly, the selectivities toward H_2 at temperatures higher than *ca.* 500 °C are similar to those obtained in the absence of butane in the feed and even higher at lower temperatures (Fig. 17C). Similar to what was observed for the Rh/Al_2O_3 and Ru/Al_2O_3 catalysts discussed above, the selectivities toward CO and CO_2 are not affected appreciably by the presence of butane (Fig. 17D).

As shown in Fig. 18, the Ru/CeO_2-ZrO_2 catalyst exhibits excellent stability with time-on-stream at 550 °C using the 85:15 mixture in the feed. In particular, after a period of *ca.* 5 h the conversions of propane and butane are stabilized at *ca.* 38% and 62%, respectively, and do not further change up to the end of the experiment. In addition, the catalyst is highly selective toward H_2 and CO_2, with S_{H2} and S_{CO2} acquiring values of *ca.* 90% and 75%, respectively, throughout the run.

The excellent stability of the Ru/CeO_2-ZrO_2 catalyst is reflected in the type and amount of carbon species accumulated on the catalyst surface. As shown in Fig. 14 (trace d), the TPO profile obtained over this sample after the stability test is characterized by the presence of a single and relatively very small CO_2 peak centered at 265 °C. As discussed above, this peak can be attributed to C_α species located in the vicinity of the dispersed metal crystallites. These species are highly reactive and can be easily gasified at reaction conditions, which is evidenced by the absence of TPO peaks at higher temperatures. In addition, the amount of accumulated carbon (1.5 mg C g_{cat}^{-1}) is more than one order of magnitude lower than that obtained for the Rh/Al_2O_3 and Ru/Al_2O_3 catalysts discussed above. The same trend is observed when the amount of accumulated carbon is expressed per mol of reacted hydrocarbons (Table 3). It is evident that the combination of Ru with the CeO_2-ZrO_2 support provides an active, selective and very stable catalyst for the steam reforming of LPG.

4. Conclusions

The steam reforming (SR) of propane and LPG (propane-butane mixtures) has been investigated over supported metal catalysts to study the effects of the nature of the dispersed metallic phase (Ru, Rh, Ir, Pt, Pd, Re) and the support (Al_2O_3, TiO_2, CeO_2-ZrO_2) on the catalytic performance and resistance against carbon accumulation. Results obtained are summarized as follows:

(1) The catalytic activity of the Al_2O_3-supported catalysts (1 wt% metal loading) for the propane SR reaction decreases in the order Ru~Rh>Ir>Pt>Pd>Re. The Ru and Rh catalysts are characterized by high propane conversions and high selectivities toward H_2, which are comparable to those of the reference 10%Ni/Al_2O_3 catalyst. The propane conversion curve is not significantly different when Rh is supported on TiO_2, compared to Al_2O_3, but shifts toward higher temperatures when dispersed on CeO_2-ZrO_2. In contrast, the catalytic performance of Ru does not vary appreciably when supported on Al_2O_3, TiO_2 or CeO_2-ZrO_2.

(2) Results of stability tests performed under propane SR reaction conditions at 600 °C for 40 h show that the catalytic performance of the 10%Ni/Al_2O_3 and Rh/Al_2O_3 catalysts deteriorates with time-on-stream due to the accumulation of relatively large amounts of less reactive carbon species, such as polymeric carbon (C_β). This is more pronounced for the 10%Ni catalyst, which also favors the formation of vermicular carbon species (CV). In contrast, the Ru/Al_2O_3 and Ru/CeO_2-ZrO_2 catalysts exhibit a relatively very stable performance and are characterized by the accumulation of much lower amounts of carbon, mainly in the form of monoatomic carbon (C_α), which can be gasified in TPO experiments at significantly lower temperatures (< 450 °C) compared to the Rh and, especially, the 10%Ni catalyst. The high stability of the Ru/CeO_2-ZrO_2 catalyst and its ability to accumulate very small amounts of easily oxidizable carbon (< 300 °C) on its surface has been attributed to the redox properties of the CeO_2-ZrO_2 support and the availability of highly labile lattice oxygen species under SR reaction conditions.

(3) Results of catalytic performance tests obtained for the SR of LPG over Rh/Al_2O_3, Ru/Al_2O_3 and Ru/CeO_2-ZrO_2 samples using concentrated feeds show that the presence of butane in the feed inhibits propane conversion because it adsorbs more strongly on the catalyst surface and that conversion of butane is generally higher than that of propane in the temperature range investigated. Similar to what was observed in the absence of butane in the feed, stability tests performed under LPG reforming reaction conditions at 550 °C for 40 h show that the two Ru-containing samples are more stable, compared to Rh/Al_2O_3. This has been attributed to the different types and amounts of accumulated coke species on the catalyst surfaces. In particular, results of TPO experiments indicate the presence of three kinds of carbon deposits (C_α, C_β, and graphitic) on the surface of the Rh/Al_2O_3 catalyst. In contrast, the Ru/Al_2O_3 catalyst forms mainly C_α and relatively small amounts of inactive graphitic carbon. Finally, the TPO profile obtained for the Ru/CeO_2-ZrO_2 sample reveals the presence of a single and relatively very small CO_2 peak centered at 265 °C, attributed to reactive C_α species located in the vicinity of the dispersed Ru crystallites.

(4) The catalytic performance of dispersed metal catalysts for the steam reforming of propane and LPG depends strongly on the nature of both the metallic phase and the support. Best results were obtained for the Ru/CeO_2-ZrO_2 catalyst, which is characterized by high activity, high selectivity toward H_2, and excellent stability with time-on-stream. This has been attributed to the comparably higher efficiency of Ru to gasify carbon deposits under reaction conditions which, when combined with the favorable redox properties of the CeO_2-ZrO_2 support, results in the suppression of carbon accumulation on the catalyst surface.

CRediT authorship contribution statement

T.R., V.E. and G.K. contributed to sample preparation and carried out the experiments. T.R. and D.K. contributed to the interpretation of the results and wrote the manuscript. D.K. conceived the original idea and supervised the project.

Declaration of Competing Interest

The authors declare that they have no known competing financial interests or personal relationships that could have appeared to influence the work reported in this paper.

Acknowledgments

The assistance of Dr. Ioanna Papavasileiou, Post-Doctoral Researcher at FORTH/ICE-HT and at the Department of Chemical Engineering of the University of Patras, Greece, in measuring hydrogen chemisorption with the volumetric method is gratefully acknowledged.

This research has been co-financed by the European Union and Greek National Funds through the Operational Program Competitiveness, Entrepreneurship, and Innovation, under the call RESEARCH-CREATE-INNOVATE (project code: T1EDK-02442).

Appendix A. Supplementary material

Supplementary data associated with this article can be found in the online version at doi:10.1016/j.apcatb.2022.121129.

References

[1] J.D. Holladay, J. Hu, D.L. King, Y. Wang, An overview of hydrogen production technologies, Catal. Today 139 (2009) 244–260, https://doi.org/10.1016/j.cattod.2008.08.039.

[2] S. Chen, C. Pei, J. Gong, Insights into interface engineering in steam reforming reactions for hydrogen production, Energy Environ. Sci. 12 (2019) 3473–3495, https://doi.org/10.1039/C9EE02808K.

[3] R.Y. Kannah, S. Kavitha, O.P.Karthikeyan Preethi, G. Kumar, N.Vo Dai-Viet, J. R. Banu, Techno-economic assessment of various hydrogen production methods – a review, Bioresour. Technol. 319 (2021), 124175, https://doi.org/10.1016/j.biortech.2020.124175.

[4] J.-C. Martin, P. Millington, B. Campbell, L. Barron, S. Fisher, On-board generation of hydrogen to improve in-cylinder combustion and after-treatment efficiency and emissions performance of a hybrid hydrogen-gasoline engine, Int. J. Hydrog. Energy 44 (2019) 12880–12889, https://doi.org/10.1016/j.ijhydene.2018.12.164.

[5] R.L. Edwards, C. Font-Palma, J. Howe, The status of hydrogen technologies in the UK: a multi-disciplinary review, Sustain. Energy Technol. Assess. 43 (2021), 100901, https://doi.org/10.1016/j.seta.2020.100901.

[6] R.-A. Felseghi, E. Carcadea, M.S. Raboaca, C.N. Trufin, C. Filote, Hydrogen fuel cell technology for the sustainable future of stationary applications, Energies 12 (2019) 4593, https://doi.org/10.3390/en12234593.

[7] A.G. Olabi, T. Wilberforce, M.A. Abdelkareem, Fuel cell application in the automotive industry and future perspective, Energy 214 (2021), 118955, https://doi.org/10.1016/j.energy.2020.118955.

[8] P. Nikolaidis, A. Poullikkas, A comparative overview of hydrogen production processes, Renew. Sustain. Energy Rev. 67 (2017) 597–611, https://doi.org/10.1016/j.rser.2016.09.044.

[9] T.L. LeValley, A.R. Richard, M. Fan, The progress in water gas shift and steam reforming hydrogen production technologies – a review, Int. J. Hydrog. Energy 39 (2014) 16983–17000, https://doi.org/10.1016/j.ijhydene.2014.08.041.

[10] J. Lui, W.-H. Chen, D.C.W. Tsang, S. You, A critical review on the principles, applications, and challenges of waste-to-hydrogen technologies, Renew. Sustain. Energy Rev. 134 (2020), 110365, https://doi.org/10.1016/j.rser.2020.110365.

[11] R. Kumar, V. Strezov, Thermochemical production of bio-oil: a review of downstream processing technologies for bio-oil upgrading, production of hydrogen and high value-added products, Renew. Sustain. Energy Rev. 135 (2021), 110152, https://doi.org/10.1016/j.rser.2020.110152.

[12] Z. Chen, W. Wei, B.-J. Ni, Cost-effective catalysts for renewable hydrogen production via electrochemical water splitting: Recent advances, Curr. Opin. Green Sustain. Chem. 27 (2021), 100398, https://doi.org/10.1016/j.cogsc.2020.100398.

[13] Y. Xu, C. Wang, Y. Huang, J. Fu, Recent advances in electrocatalysts for neutral and large-current-density water electrolysis, Nano Energy 80 (2021), 105545, https://doi.org/10.1016/j.nanoen.2020.105545.

[14] R.P. Borges, L.G. Moura, J.J. Spivey, F.B. Noronha, C.E. Hori, Hydrogen production by steam reforming of LPG using supported perovskite type precursors, Int. J. Hydrog. Energy 45 (2020) 21166–21177, https://doi.org/10.1016/j.ijhydene.2020.05.183.

[15] M. Tonezzer, T.T. Le Dang, Q.H. Tran, V.H. Nguyen, S. Iannotta, Selective hydrogen sensor for liquefied petroleum gas steam reforming fuel cell systems, Int. J. Hydrog. Energy 42 (2017) 740–748, https://doi.org/10.1016%2Fj.ijhydene.2016.11.102.

[16] B. Silberova, H.J. Venvik, Anders Holmen, Production of hydrogen by short contact time partial oxidation and oxidative steam reforming of propane, Catal. Today 99 (2005) 69–76, https://doi.org/10.1016/j.cattod.2004.09.025.

[17] X. Zou, X. Wang, L. Li, K. Shen, X. Lu, W. Ding, Development of highly effective supported nickel catalysts for pre-reforming of liquefied petroleum gas under low

steam to carbon molar ratios, Int. J. Hydrog. Energy 35 (2010) 12191–12200, https://doi.org/10.1016/j.ijhydene.2010.08.080.
[18] P.P. Silva, R.A. Ferreira, J.F. Nunes, J.A. Sousa, L.L. Romanielo, F.B. Noronha, C. E. Hori, Production of hydrogen from the steam and oxidative reforming of LPG: thermodynamic and experimental study, Braz. J. Chem. Eng. 32 (2015) 647–662, https://doi.org/10.1590/0104-6632.20150323s00003441.
[19] Y. Im, J.H. Lee, B.S. Kwak, J.Y. Do, M. Kang, Effective hydrogen production from propane steam reforming using M/NiO/YSZ catalysts (M = Ru, Rh, Pd, and Ag), Catal. Today 303 (2018) 168–176, https://doi.org/10.1016/j.cattod.2017.08.056.
[20] R. Arvaneh, A.A. Fard, A. Bazyari, S.M. Alavi, F.J. Abnavi, Effects of Ce, La, Cu, and Fe promoters on Ni/$MgAl_2O_4$ catalysts in steam reforming of propane, Korean J. Chem. Eng. 36 (2019) 1033–1041, https://doi.org/10.1007/s11814-019-0295-x.
[21] R.A.R. Ferreira, C.N. Ávila-Neto, F.B. Noronha, C.E. Hori, Study of LPG steam reform using Ni/Mg/Al hydrotalcite-type precursors, Int. J. Hydrog. Energy 44 (2019) 24471–24484, https://doi.org/10.1016/j.ijhydene.2019.07.193.
[22] K.J. Morganti, T.M. Foong, M.J. Brear, G. da Silva, Y. Yang, F.L. Dryer, The research and motor octane numbers of liquefied petroleum gas (LPG), Fuel 108 (2013) 797–811, https://doi.org/10.1016/j.fuel.2013.01.072.
[23] G. Kolb, R. Zapf, V. Hessel, H. Löwe, Propane steam reforming in micro-channels-results from catalyst screening and optimisation, Appl. Catal. A 277 (2004) 155–166, https://doi.org/10.1016/j.apcata.2004.09.007.
[24] C. Resini, M.C. Herrera Delgado, L. Arrighi, L.J. Alemany, R. Marazza, G. Busca, Propene versus propane steam reforming for hydrogen production over Pd-based and Ni-based catalysts, Catal. Commun. 6 (2005) 441–445, https://doi.org/10.1016/j.catcom.2005.03.009.
[25] S. Natesakhawat, R.B. Watson, X. Wang, U.S. Ozkan, Deactivation characteristics of lanthanide-promoted sol–gel Ni/Al_2O_3 catalysts in propane steam reforming, J. Catal. 234 (2005) 496–508, https://doi.org/10.1016/j.jcat.2005.07.014.
[26] W.C. Chueh, Z. Shao, S.M. Haile, Tunability of propane conversion over alumina supported Pt and Rh catalysts, Top. Catal. 46 (2007) 402–411, https://doi.org/10.1007/s11244-007-9012-9.
[27] H.-J. Lee, Y.-S. Lim, N.-C. Park, Y.-C. Kim, Catalytic autothermal reforming of propane over the noble metal-doped hydrotalcite-type catalysts, Chem. Eng. J. 146 (2009) 295–301, https://doi.org/10.1016%2Fj.cej.2008.10.007.
[28] R. Zapf, R. Thiele, M. Wichert, M. O'Connell, A. Ziogas, G. Kolb, Application of rhodium nanoparticles for steam reforming of propane in microchannels, Catal. Commun. 41 (2013) 140–145, https://doi.org/10.1016/j.catcom.2013.07.018.
[29] T. Hou, B. Yu, S. Zhang, J. Zhang, D. Wang, T. Xu, L. Cui, W. Cai, Hydrogen production from propane steam reforming over Ir/$Ce_{0.75}Zr_{0.25}O_2$ catalyst, Appl. Catal. B 168–169 (2015) 524–530, https://doi.org/10.1016%2Fj.apcatb.2015.01.023.
[30] Y. Li, X. Wang, C. Song, Spectroscopic characterization and catalytic activity of Rh supported on CeO_2-modified Al_2O_3 for low-temperature steam reforming of propane, Catal. Today 263 (2016) 22–34, https://doi.org/10.1016/j.cattod.2015.08.063.
[31] L. Yu, K. Sato, T. Toriyama, T. Yamamoto, S. Matsumura, K. Nagaoka, Influence of the crystal structure of titanium oxide on the catalytic activity of Rh/TiO_2 in steam reforming of propane at low temperature, Chem. Eur. J. 24 (2018) 8742–8746, https://doi.org/10.1002/chem.201800936.
[32] L. Yu, K. Sato, K. Nagaoka, Rh/$Ce_{0.25}Zr_{0.75}O_2$ catalyst for steam reforming of propane at low temperature, ChemCatChem 11 (2019) 1472–1479, https://doi.org/10.1002/cctc.201801824.
[33] A. Kokka, A. Katsoni, I.V. Yentekakis, P. Panagiotopoulou, Hydrogen production via steam reforming of propane over supported metal catalysts, Int. J. Hydrog. Energy 45 (2020) 14849–14866, https://doi.org/10.1016/j.ijhydene.2020.03.194.
[34] D.J. Moon, Hydrogen production by catalytic reforming of gaseous hydrocarbons (methane & LPG), Catal. Surv. Asia 12 (2008) 188–202, https://doi.org/10.1007/s10563-008-9051-7.
[35] J.H. Park, D. Lee, H.C. Lee, E.D. Park, Steam reforming of liquid petroleum gas over Mn-promoted Ni/γ-Al_2O_3 catalysts, Korean J. Chem. Eng. 27 (2010) 1132–1138, https://doi.org/10.1007/s11814-010-0212-9.
[36] N. Laosiripojana, W. Sutthisripok, S. Charojrochkul, S. Assabumrungrat, Steam reforming of LPG over Ni and Rh supported on Gd-CeO_2 and Al_2O_3: Effect of support and feed composition, Fuel 90 (2011) 136–141, https://doi.org/10.1016/j.fuel.2010.07.053.
[37] Z.O. Malaibari, A. Amin, E. Croiset, W. Epling, Performance characteristics of Mo-Ni/Al_2O_3 catalysts in LPG oxidative steam reforming for hydrogen production, Int. J. Hydrog. Energy 39 (2014) 10061–10073, https://doi.org/10.1016/j.ijhydene.2014.03.169.
[38] E.C. Faria, R.C. Rabelo-Neto, R.C. Colman, R.A.R. Ferreira, C.E. Hori, F.B. Noronha, Steam reforming of LPG over Ni/Al_2O_3 and Ni/$Ce_xZr_{1-x}O_2$/Al_2O_3 catalysts, Catal. Lett. 146 (2016) 2229–2241. ⟨https://link.springer.com/article/10.1007/s10562-016-1833-3⟩.
[39] P.P. Silva, R.A.R. Ferreira, F.B. Noronha, C.E. Hori, Hydrogen production from steam and oxidative steam reforming of liquefied petroleum gas over cerium and strontium doped $LaNiO_3$ catalysts, Catal. Today 289 (2017) 211–221, https://doi.org/10.1016/j.cattod.2016.10.003.
[40] D.M. Lohan, C.C. Cormos, Evaluation of hydrogen production from catalytic reforming of liquefied petroleum gas with carbon capture and storage, Stud. Univ. Babes-Bolyai Chem. 62 (2017) 241–252, https://doi.org/10.24193/subbchem.2017.4.21.
[41] C.N. Ávila-Neto, K.D. Oliveira, K.F. Oliveira, A.M.M. Arouca, R.A.R. Ferreira, C. E. Hori, Interconnection between feed composition and Ni/Co ratio in (La-Ni-Co-O)-based perovskites and its effects on the stability of LPG steam reforming, Appl. Catal. A Gen. 550 (2018) 184–197, https://doi.org/10.1016/j.apcata.2017.11.011.
[42] L.G. Moura, R.P. Borges, F.B. Noronha, C.E. Hori, Steam reforming of liquefied petroleum gas using catalysts supported on ceria-silica, Int. J. Hydrog. Energy 46 (2021) 1801–1814, https://doi.org/10.1016/j.ijhydene.2020.10.021.
[43] D.L. Trimm, Coke formation and minimisation during steam reforming reactions, Catal. Today 37 (1997) 233–238, https://doi.org/10.1016/S0920-5861(97)00014-X.
[44] P. Alphonse, F. Ansart, Catalytic coatings on steel for low-temperature propane prereforming to solid oxide fuel cell (SOFC) application, J. Colloid Interface Sci. 336 (2009) 658–666, https://doi.org/10.1016/j.jcis.2009.04.079.
[45] X. Wang, R.J. Gorte, A study of steam reforming of hydrocarbon fuels on Pd/ceria, Appl. Catal. A 224 (2002) 209–218, https://doi.org/10.1016/S0926-860X(01)00783-9.
[46] P. Panagiotopoulou, D.I. Kondarides, Effect of morphological characteristics of TiO_2-supported noble metal catalysts on their activity for the water-gas shift reaction, J. Catal. 225 (2004) 327–336, https://doi.org/10.1016/j.jcat.2004.04.030.
[47] A. Petala, D. Tsikritzis, M. Kollia, S. Ladas, S. Kennou, D.I. Kondarides, Synthesis and characterization of N-doped TiO_2 photocatalysts with tunable response to solar radiation, Appl. Surf. Sci. 305 (2014) 281–291, https://doi.org/10.1016/j.apsusc.2014.03.062.
[48] A. Kotsifa, T.I. Halkides, D.I. Kondarides, X.E. Verykios, Activity enhancement of bimetallic Rh-Ag/Al_2O_3 catalysts for selective catalytic reduction of NO by C_3H_6, Catal. Lett. 79 (2002) 113–117, https://doi.org/10.1023/A:1015308408840.
[49] S.S. Akarmazyan, P. Panagiotopoulou, A. Kambolis, Ch Papadopoulou, D. I. Kondarides, Methanol dehydration to dimethylether over Al_2O_3 catalysts, Appl. Catal. B 145 (2014) 136–148, https://doi.org/10.1016/j.apcatb.2012.11.043.
[50] I.V. Yentekakis, G. Goula, M. Hatzisymeon, I. Betsi-Argyropoulou, G. Botzolaki, K. Kousi, D.I. Kondarides, M.J. Taylor, Ch.M.A. Parlett, A. Osatiashtiani, G. Kyriakou, J.P. Holgado, R.M. Lambert, Effect of support oxygen storage capacity on the catalytic performance of Rh nanoparticles in the CO_2 reforming of methane, Appl. Catal. B 243 (2019) 490–501, https://doi.org/10.1016/j.apcatb.2018.10.048.
[51] T. Ramantani, G. Bampos, A. Vavatsikos, G. Vatskalis, D.I. Kondarides, Propane steam reforming over catalysts derived from noble metal (Ru, Rh)-substituted $LaNiO_3$ and $La_{0.8}Sr_{0.2}NiO_3$ perovskite precursors, Nanomaterials 11 (2021) 1931, https://doi.org/10.3390/nano11081931.
[52] A.N. Fatsikostas, D.I. Kondarides, X.E. Verykios, Production of hydrogen for fuel cells by reformation of biomass-derived ethanol, Catal. Today 75 (2002) 145–155, https://doi.org/10.1016/S0920-5861(02)00057-3.
[53] T.I. Halkides, D.I. Kondarides, X.E. Verykios, Catalytic reduction of NO by C_3H_6 over Rh/TiO_2 catalysts. Effect of W^{6+}-cation doping of TiO_2 on morphological characteristics and catalytic performance, Appl. Catal. B 41 (2003) 415–426, https://doi.org/10.1016/S0926-3373(02)00176-5.
[54] M.D. Argyle, C.H. Bartholomew, Heterogeneous catalyst deactivation and regeneration: a review, Catalysts 5 (2015) 145–269, https://doi.org/10.3390/catal5010145.
[55] S. Ewald, S. Standl, O. Hinrichsen, Characterization of nickel catalysts with transient methods, Appl. Catal. A 549 (2018) 93–101, https://doi.org/10.1016/j.apcata.2017.09.023.
[56] K.N. Papageridis, N.D. Charisiou, S.L. Douvartzides, V. Sebastian, S.J. Hinder, M. A. Baker, S. AlKhoori, K. Polychronopoulou, M.A. Goula, Effect of operating parameters on the selective catalytic deoxygenation of palm oil to produce renewable diesel over Ni supported on Al_2O_3, ZrO_2 and SiO_2 catalysts, Fuel Process. Technol. 209 (2020), 106547, https://doi.org/10.1016/j.fuproc.2020.106547.
[57] C. Amorim, M.A. Keane, Catalytic hydrodechlorination of chloroaromatic gas streams promoted by Pd and Ni: The role of hydrogen spillover, J. Hazard. Mater. 211– (212) (2012) 208–217, https://doi.org/10.1016/j.jhazmat.2011.08.025.
[58] F. Benseradj, F. Sadi, M. Chater, Hydrogen spillover studies on diluted Rh/Al_2O_3 catalyst, Appl. Catal. A 228 (2002) 135–144, https://doi.org/10.1016/S0926-860X(01)00971-1.
[59] R. Kramer, M. Andre, Adsorption of atomic hydrogen on alumina by hydrogen spillover, J. Catal. 58 (1979) 287–295, https://doi.org/10.1016/0021-9517(79)90266-5.
[60] G. Zhou, B. Dai, H. Xie, G. Zhang, K. Xiong, X. Zheng, CeCu composite catalyst for CO synthesis by reverse water–gas shift reaction: effect of Ce/Cu mole ratio, J. CO2 Util. 21 (2017) 292–301, https://doi.org/10.1016/j.jcou.2017.07.004.
[61] S. Bernal, J.J. Calvino, G.A. Cifredo, J.M. Rodriguez-Izquierdo, V. Perrichon, A. Laachir, Reversibility of hydrogen chemisorption on a ceria-supported rhodium catalyst, J. Catal. 137 (1992) 1–11, https://doi.org/10.1016/0021-9517(92)90134-4.
[62] E.W. Shin, S.-I. Cho, J.H. Kang, W.J. Kim, J.D. Park, S.H. Moon, Palladium-hydrogen interaction on supported palladium catalysts of different metal dispersions, Korean J. Chem. Eng. 17 (2000) 468–472, https://doi.org/10.1007/BF02706862.
[63] A.-G. Boudjahem, A. Redjel, T. Mokrane, Preparation, characterization and performance of Pd/SiO_2 catalyst for benzene catalytic hydrogenation, J. Ind. Eng. Chem. 18 (2012) 303–308, https://doi.org/10.1016/j.jiec.2011.11.038.
[64] J.R. Rostrup-Nielsen, Activity of nickel catalysts for steam reforming of hydrocarbons, J. Catal. 31 (1973) 173–199, https://doi.org/10.1016/0021-9517(73)90326-6.
[65] D. Qin, J. Lapszewicz, Study of mixed steam and CO_2 reforming of CH_4 to syngas on MgO-supported metals, Catal. Today 21 (1994) 55l–560l, https://doi.org/10.1016/0920-5861(94)80179-7.
[66] G. Jones, J.G. Jakobsen, S.S. Shim, J. Kleisa, M.P. Andersson, J. Rossmeisl, F. Abild-Pedersen, T. Bligaard, S. Helveg, B. Hinnemann, J.R. Rostrup-Nielsen,

I. Chorkendorff, J. Sehested, J.K. Nørskov, First principles calculations and experimental insight into methane steam reforming over transition metal catalysts, J. Catal. 259 (2008) 147–160, https://doi.org/10.1016/j.jcat.2008.08.003.

[67] P. Panagiotopoulou, D.I. Kondarides, X.E. Verykios, Selective methanation of CO over supported noble metal catalysts: Effects of the nature of the metallic phase on catalytic performance, Appl. Catal. A 344 (2008) 45–54, https://doi.org/10.1016/j.apcata.2008.03.039.

[68] P. Panagiotopoulou, D.I. Kondarides, X.E. Verykios, Chemical reaction engineering and catalysis issues in distributed power generation systems, Ind. Eng. Chem. Res. 50 (2011) 523–530, https://doi.org/10.1021/ie100132g.

[69] X. Cui, S.K. Kær, Thermodynamic analysis of steam reforming and oxidative steam reforming of propane and butane for hydrogen production, Int. J. Hydrog. Energy 43 (2018) 13009–13021, https://doi.org/10.1016/j.ijhydene.2018.05.083.

[70] D.L. Trimm, Catalysts for the control of coking during steam reforming, Catal. Today 49 (1999) 3–10, https://doi.org/10.1016/S0920-5861(98)00401-5.

[71] N.D. Charisiou, G.I. Siakavelas, B. Dou, V. Sebastian, S.J. Hinder, M.A. Baker, K. Polychronopoulou, M.A. Goula, Nickel supported on $AlCeO_3$ as a highly selective and stable catalyst for hydrogen production via the glycerol steam reforming reaction, Catalysts 9 (2019) 411, https://doi.org/10.3390/catal9050411.

[72] M. Rezaei, S.M. Alavi, S. Sahebdelfar, Z.-F. Yan, Syngas production by methane reforming with carbon dioxide on noble metal catalysts, J. Nat. Gas Chem. 15 (2006) 327–334, https://doi.org/10.1016/S1003-9953(07)60014-0.

[73] F.B. Noronha, E.C. Fendley, R.R. Soares, W.E. Alvarez, D.E. Resasco, Correlation between catalytic activity and support reducibility in the CO_2 reforming of methane over $Pt/Ce_xZr_{1-x}O_2$ catalysts, Chem. Eng. J. 82 (2001) 21–31, https://doi.org/10.1016/S1385-8947(00)00368-5.

[74] J.R. Rostrup-Nielsen, J. Sehested, J.K. Nørskov, Hydrogen and synthesis gas by steam- and CO_2 reforming, Adv. Catal. 47 (2002) 65–139, https://doi.org/10.1016/S0360-0564(02)2947006-X.